


ATMOSPHERIC MOISTURE TRANSPORT AND ITS IMPACT ON THE WATER
CYCLE OVER ALASKA AND HAWAII: THE ROLES OF THE PACIFIC DECADEAL
OSCILLATION AND EL NIÑO

By


Cecilia J. Borries

RECOMMENDED:



Uma Bhatt

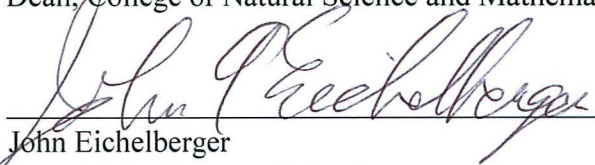

Nicole Mölders

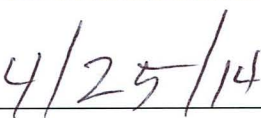

Xiangdong Zhang
Advisory Committee Chair


Uma Bhatt
Chair, Department of Atmospheric Sciences

APPROVED:


Paul Layer
Dean, College of Natural Science and Mathematics


John Eichelberger
Dean of the Graduate School


Date

ATMOSPHERIC MOISTURE TRANSPORT AND ITS IMPACT ON THE WATER
CYCLE OVER ALASKA AND HAWAII: THE ROLES OF THE PACIFIC DECADAL
OSCILLATION AND EL NIÑO

A
THESIS

Presented to the Faculty
of the University of Alaska Fairbanks

in Partial Fulfillment of the Requirements
for the Degree of

MASTER OF SCIENCE

By
Cecilia J. Borries, B. S.

Fairbanks, Alaska

May 2014

Abstract

Precipitation over the North Pacific can fluctuate under climate patterns such as the Pacific Decadal Oscillation (PDO) and El Niño-Southern Oscillation (ENSO). In order to better understand the role which these climatic patterns play in the North Pacific water budgets and pathways, we employed the Community Atmosphere Model 5.0 (CAM) and conducted sensitivity experiments to examine how atmospheric moisture convergence and moisture transport respond to sea surface temperature (SST) anomalies associated with the PDO and ENSO phase transitions. We have found that changes in transient moisture transport, as the PDO phase shifts from cool to warm, are due to increases in specific humidity and decreases in wind speeds over Alaska and the North Pacific. Additionally, increases in moisture convergence, specific humidity, and wind speeds and decreases in transient moisture transport are seen over the North Pacific during El Niño events compared to La Niña events.

Table of Contents

	Page
Signature Page	i
Title Page	iii
Abstract	v
Table of Contents	vii
List of Figures	ix
List of Tables	xi
Acknowledgements	xiii
Chapter 1 Introduction	1
1.1 Motivation	1
1.2 Previous Research	2
1.3 Pacific Decadal Oscillation	3
1.4 El Niño	5
Chapter 2 Model Information	9
2.1 Model Specifications	9
2.2 Model Verification	10
2.3 PDO Experiment	16
2.4 PDO and ENSO Experiment	16
2.5 Data	17
Chapter 3 Results of the PDO Sensitivity Experiment	19
3.1 Precipitation	19

	Page
3.2 Moisture Convergence	29
3.3 Moisture Transport.....	32
3.4 Specific Humidity and Wind	46
3.5 Evaporation.....	50
Chapter 4 Results of the PDO and El Niño Experiment.....	53
4.1 Moisture Convergence	53
4.2 Moisture Transport.....	56
4.3 Specific Humidity and Wind	59
4.4 Evaporation.....	64
Chapter 5 Summary and Conclusions.....	67
References.....	73

List of Figures

	Page
Figure 1.1: PDO SST, wind, and SLP anomalies	4
Figure 1.2: El Niño sea level anomalies	6
Figure 1.3: PDO Index and Niño3.4 Index timeseries.....	7
Figure 2.1: Model verification of mean specific humidity	11
Figure 2.2: Model verification of mean sea level pressure.....	12
Figure 2.3: Model verification of mean geopotential height at 500mb	13
Figure 2.4: Model verification of mean wind at 850mb	14
Figure 2.5: Model verification of mean wind at 500mb	15
Figure 2.6: SST forcing for CAM5.....	17
Figure 3.1: Winter accumulated precipitation	20
Figure 3.2: Spring accumulated precipitation.....	21
Figure 3.3: Summer accumulated precipitation	22
Figure 3.4: Fall accumulated precipitation	23
Figure 3.5: PDO difference of accumulated precipitation	28
Figure 3.6: PDO difference of moisture convergence	31
Figure 3.7: PDO difference of mean moisture transport.....	34
Figure 3.8: PDO difference of term 2 in Equation 3.5.....	35
Figure 3.9: PDO difference of term 3 in Equation 3.5.....	36
Figure 3.10: PDO difference of transient moisture transport	38
Figure 3.11: Boundaries for net transport calculation	39

	Page
Figure 3.12: Seasonal net moisture transport into Alaska	40
Figure 3.13: Seasonal net moisture transport across east boundary	42
Figure 3.14: Seasonal net moisture transport across north boundary	43
Figure 3.15: Seasonal net moisture transport across west boundary	44
Figure 3.16: Seasonal net moisture transport across south boundary	45
Figure 3.17: PDO difference in precipitable water	48
Figure 3.18: PDO difference in mass flux	49
Figure 3.19: PDO difference in evaporation.....	51
Figure 4.1: PDO difference in moisture convergence during La Niña.....	54
Figure 4.2: PDO difference in moisture convergence during El Niño	55
Figure 4.3: PDO difference in transient moisture transport during La Niña	57
Figure 4.4: PDO difference in transient moisture transport during El Niño.....	58
Figure 4.5: PDO difference in precipitable water during La Niña	60
Figure 4.6: PDO difference in precipitable water during El Niño.....	61
Figure 4.7: PDO difference in mass flux during La Niña.....	62
Figure 4.8: PDO difference in mass flux during El Niño	63
Figure 4.9: PDO difference in evaporation during La Niña	65
Figure 4.10: PDO difference in evaporation during El Niño.....	66
Figure 5.1: Model topography over the North Pacific Ocean.....	68
Figure 5.2: Topography of Alaska.....	68

List of Tables

	Page
Table 3.1: Mean Observed Winter Accumulated Precipitation	24
Table 3.2: Mean Observed Spring Accumulated Precipitation	24
Table 3.3: Mean Observed Summer Accumulated Precipitation.....	25
Table 3.4: Mean Observed Fall Accumulated Precipitation.....	25
Table 3.5: Mean Observed Annual Accumulated Precipitation	26

Acknowledgements

I would like to thank my advisor as well as my committee members for their suggestions and advice regarding my research and this thesis. I would also like to thank my coworkers and fellow graduate students for their motivation and helpful discussions.

Much love and thanks go to my parents, my siblings, and my husband, Dan. I could not have made it here without your support, encouragement, phone calls, and love from thousands of miles away.

Chapter 1. Introduction

1.1 Motivation

Precipitation is an extremely critical component in everyday life, and so understanding how precipitation can fluctuate is important for many reasons. Extreme precipitation events can flood areas and cause structural and ecological damage. Conversely, too little precipitation can leave wooded areas vulnerable to forest fires, which can then cause air quality and health problems. Farmland can be adversely affected by both extremes: drought conditions kill crops and decrease crop yields, whereas flooding removes topsoil and leaves root systems unable to support the plants. Precipitation is also a large source of potable water – the only source in some areas, and any changes can be of great impact in those areas.

Precipitation is dependent upon the amount of moisture in the atmosphere, which can be influenced by moisture transport into or out of an area. In the arctic regions, the predominant source of atmospheric moisture is transported from lower latitudes. While natural and human-induced variabilities in atmospheric moisture transport, atmospheric moisture content, and precipitation have large impacts on society and ecology, there are not many studies to investigate the changes in these variables over the North Pacific Ocean and Alaska. Therefore, this study focuses on the natural climate variability of the PDO and El Niño and examines how their sea surface temperature anomalies modulate moisture transport and precipitation in this area.

1.2 Previous Research

Some changes in arctic precipitation are due to natural causes. Yarker et al. (2010) showed that high-latitude volcanic eruptions could increase or decrease precipitation in the surrounding region depending on the atmospheric conditions and the volcanic emissions (aerosols, water vapor, etc.). Additionally, heat from reoccurring summer forest fires has the ability to increase atmospheric moisture content. This extra moisture can then cause flooding in the nearby area when precipitated out but create drier conditions father away (Mölders & Kramm, 2006). Sea surface temperature anomalies in the Pacific Ocean due to natural climate variability like El Niño and the Pacific Decadal Oscillation (PDO) also impact precipitation throughout the North Pacific region (Mantua & Hare, 2002; Hartmann & Wendler, 2005).

Anthropogenic changes also affect variability in arctic precipitation. The modeling investigation of Mölders and Olson (2004) showed that recent urbanization and its corresponding urban effects in interior Alaska could have an impact on regional precipitation. Rising CO₂ concentrations and the corresponding rises in air temperatures lead to increases in precipitation around the world in another modeling experiment (Wetherald & Manabe, 2002). Evaporation from reduced sea ice concentrations in the Arctic also leads to increased moisture in the atmosphere and increased cloudiness at lower levels (Vavrus et al., 2011). Atmospheric feedbacks due to the greening of the Arctic in recent years have also been shown to increase summer precipitation (J. Zhang & Walsh, 2006).

Due to the dry nature of the Arctic, moisture transported from lower latitudes is the

main source of precipitation in Alaska. Thus, variations in moisture transport are of great importance in the study of the North Pacific water cycle. Higgins and Cassano (2009) found that precipitation has increased throughout the Arctic due to increased meridional moisture transport. Similarly, increases in poleward moisture transport over Eurasia have been documented in the observations (X. Zhang et al., 2012).

1.3 Pacific Decadal Oscillation

The Pacific Decadal Oscillation (PDO) is a source of natural climate variability in the areas surrounding the North Pacific Ocean. It is a pattern of sea surface temperature (SST) anomalies in the Pacific Ocean poleward of 20° N. It consists of two phases – a cold (negative) phase and a warm (positive) phase – and occurs on an interdecadal time scale of approximately 30 to 50 years. As seen in Figure 1.1, during a warm phase PDO, SST's in the eastern part of the Pacific Ocean (along the west coast of the United States) are warmer than average while the SST's in the western portion of the Pacific Ocean are cooler than average. The pattern reverses during the cool phase. Impacts of the PDO were first seen in salmon production along the western coasts of Alaska and Canada and the northwestern United States (Mantua et al., 1997). During the 1960's and 1970's, fisheries in Alaska were producing much less salmon than the fisheries in the Pacific Northwest (Washington, Oregon, and California). However, in the late 1970's, the productions amounts reversed. These changes coincided with other changes in the climate of the areas surrounding the Pacific Ocean and are now linked to a phase shift of the PDO: from cool to warm.

In addition to the marine ecological differences, the PDO greatly affects the

climate of the North Pacific. Greater than average temperatures occur in Alaska, in the northwestern United States, and in northwestern Australia while less than average temperatures occur in southeastern United States, Japan, and China during warm PDO phases (Mantua & Hare, 2002; Hartmann & Wendler, 2005). Precipitation in sub-arctic Alaska, western Australia, and the southwestern United States increases during warm phases and decreases in arctic Alaska, Japan, and eastern Australia (Mantua & Hare, 2002; Hartmann & Wendler, 2005). Additionally, Garza et al. (2012) have shown that the trade winds over Hawaii have shifted from northeasterly winds to easterly winds during a time period of 1973-2009, which includes a PDO phase change from cool to warm.

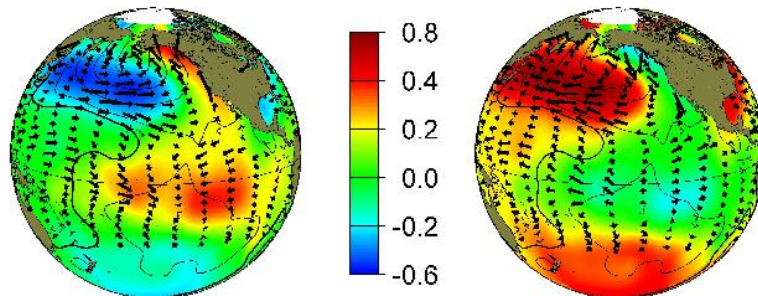


Figure 1.1. PDO SST, wind, and SLP anomalies. Anomalies for sea surface temperature are shown by color contours, wind speed by wind vectors, and surface pressure by solid contours during warm phase PDO (left) and cool phase PDO (right). Figure credit: jisao.washington.edu/pdo

1.4 El Niño Southern Oscillation

Natural climate variability in the Northern Pacific Ocean is also impacted by El Niño Southern Oscillation (ENSO). ENSO is a pattern of SST anomalies which occur in the east or central tropical Pacific Ocean between 10° S and 10° N latitude on an inter-annual time scale. Figure 1.2 depicts the sea level anomalies between El Niño and La Niña episodes. Waters with higher temperature anomalies also have higher sea level anomalies. The SST anomalies are accompanied by surface pressure anomalies in the Western Pacific Ocean (off the eastern coast of Australia). The pattern of positive SST anomalies over the Tropical Pacific is known as El Niño, and the pattern of negative SST anomalies is known as La Niña. Figure 1.3 shows both PDO and Niño3.4 indices from 1950 through 2012. Red indices indicate positive SST anomalies, while blue indices indicate negative SST anomalies. The decadal oscillation of the PDO phases and the interannual variability of El Niño and La Niña are easily seen.

Papineau (2001) has shown that El Niño episodes tend to increase wintertime temperatures in the eastern two-thirds of Alaska, while La Niña episodes decrease wintertime temperatures throughout Alaska.

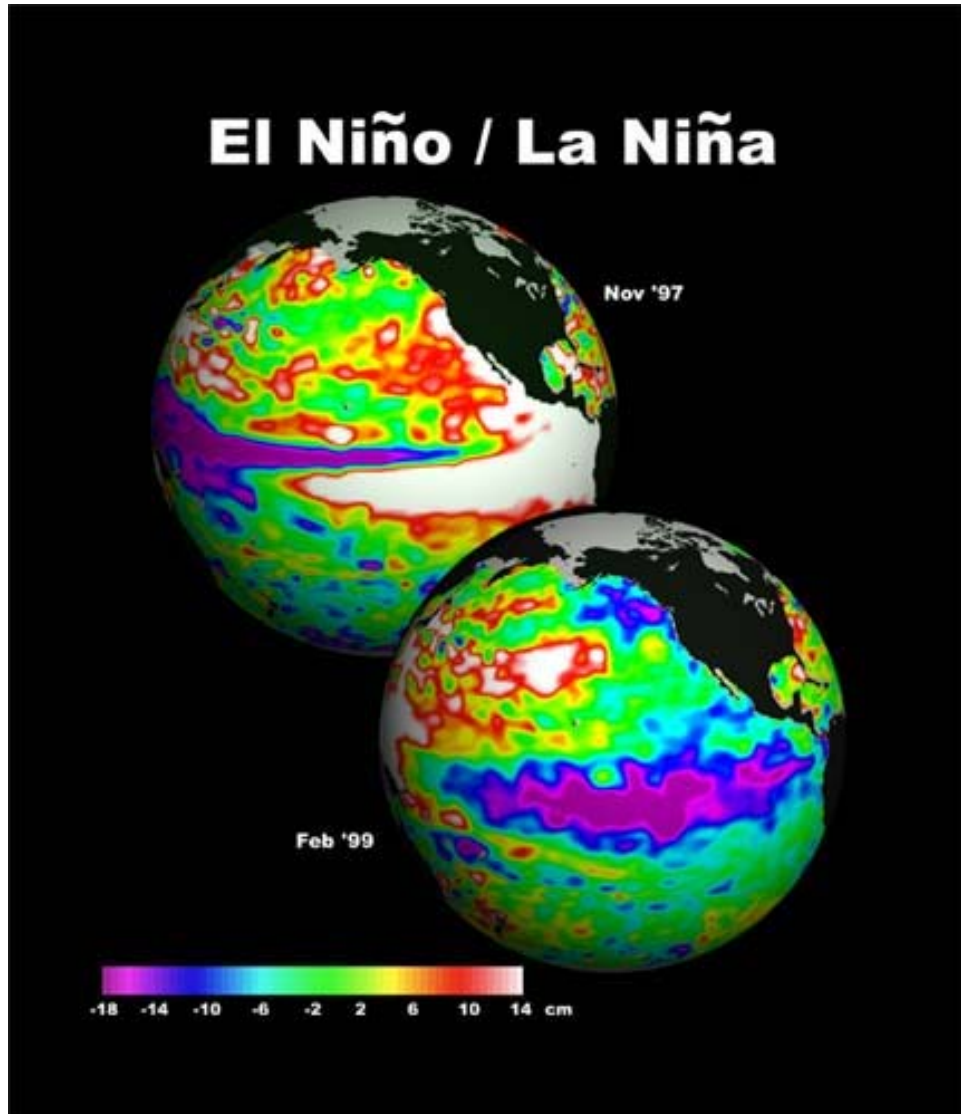


Figure 1.2. El Niño sea level anomalies. Sea level anomalies are shown by color contours for El Niño (top) and La Niña (bottom). Figure credit: ncdc.noaa.gov

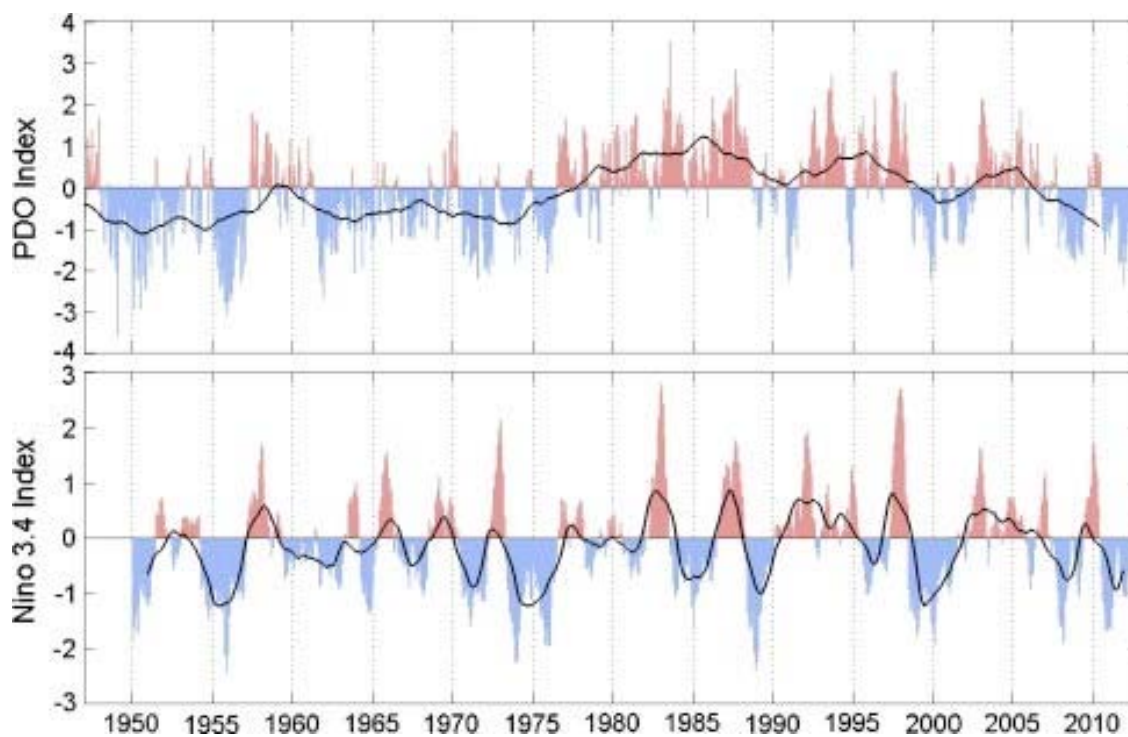


Figure 1.3. PDO Index and Niño3.4 Index timeseries. PDO indices (top) and Niño 3.4 Indices (bottom) are shown for the period 1950- 2012. Red indices indicated positive anomalies (warm phase PDO or El Niño), and blue indices indicate negative anomalies (cool phase PDO or La Niña). Figure credit: Chau-Ron Wu, Interannual modulation of the Pacific Decadal Oscillation (PDO) on the low-latitude western North Pacific, *Progress in Oceanography*, <http://dx.doi.org/10.1016/j.ocean.2012.12.001>

Chapter 2. Model Information

2.1 Model Specifications

For this study of atmospheric moisture transport over the North Pacific Ocean, the atmosphere component of the National Center for Atmospheric Research Community Earth System Model version 1.0.2 (CESM1.0.2), the Community Atmosphere Model (CAM5.0), was used in stand-alone mode. This model consists of thirty vertical levels and was run at a horizontal resolution of 0.9° by 1.25° on a finite volume grid. The finite volume dynamical core discretization is modeled after a conservative “flux form semi-Lagrangian” scheme as described by Lin and Rood (1996) and (1997) in the horizontal. In the vertical, the discretization can be considered as quasi-Lagrangian (Neale et al., 2010).

Monthly means of time-varying sea surface temperature and sea ice concentration data were used as lower-boundary forcing conditions. This data set is a blend of the HadISST1 from the Met Office Hadley Centre and version 2 of the Optimum Interpolation SST analysis, OI.v2, from the National Oceanic and Atmospheric Administration datasets, with the former spanning the years 1870-1980 and the latter 1981-2008 (Hurrell et al., 2008). Annual averages taken from the years 1981 to 2001 comprise a climatological dataset for the model.

The main hallmark of CAM5 is its improvements of cloud interaction processes which make CAM5 the first version able to model indirect radiative effects due to cloud-aerosol interactions. Additional information about CAM5 including model physics and the finite volume dynamical core can be found in Neale et al. (2010).

2.2 Model Verification

In order to verify the CAM5 model output, three year-long ensemble runs were made using the climatological SST and sea ice data boundary conditions. The monthly model output was then compared to the National Centers for Environmental Prediction – Department of Energy Reanalysis 2 (NCEP – DOE II) data at a 2° by 2° resolution and the European Center for Medium-Range Weather Forecasts (ECMWF) Reanalysis Interim (ERA – Interim) data at a 0.75° by 0.75° resolution with the following variables: specific humidity, sea level pressure, geopotential height at 500mb, and wind vectors at 850mb and 500mb. The variables were averaged over the three ensemble runs and were compared to the time averaged NCEP – DOE II and ERA – Interim data from January 1981 through December 2001 (Figures 2.1-2.5).

These comparisons show that the model output closely resembles both data sets. The model output compares better to the specific humidity, sea level pressure, and geopotential height (Figures 2.1a,b-2.3a,b) of the ERA data. Slight discrepancies exist in the wind vectors at 850mb and 500mb over Alaska between the model output and the ERA and NCEP data (Figures 2.4 and 2.5).

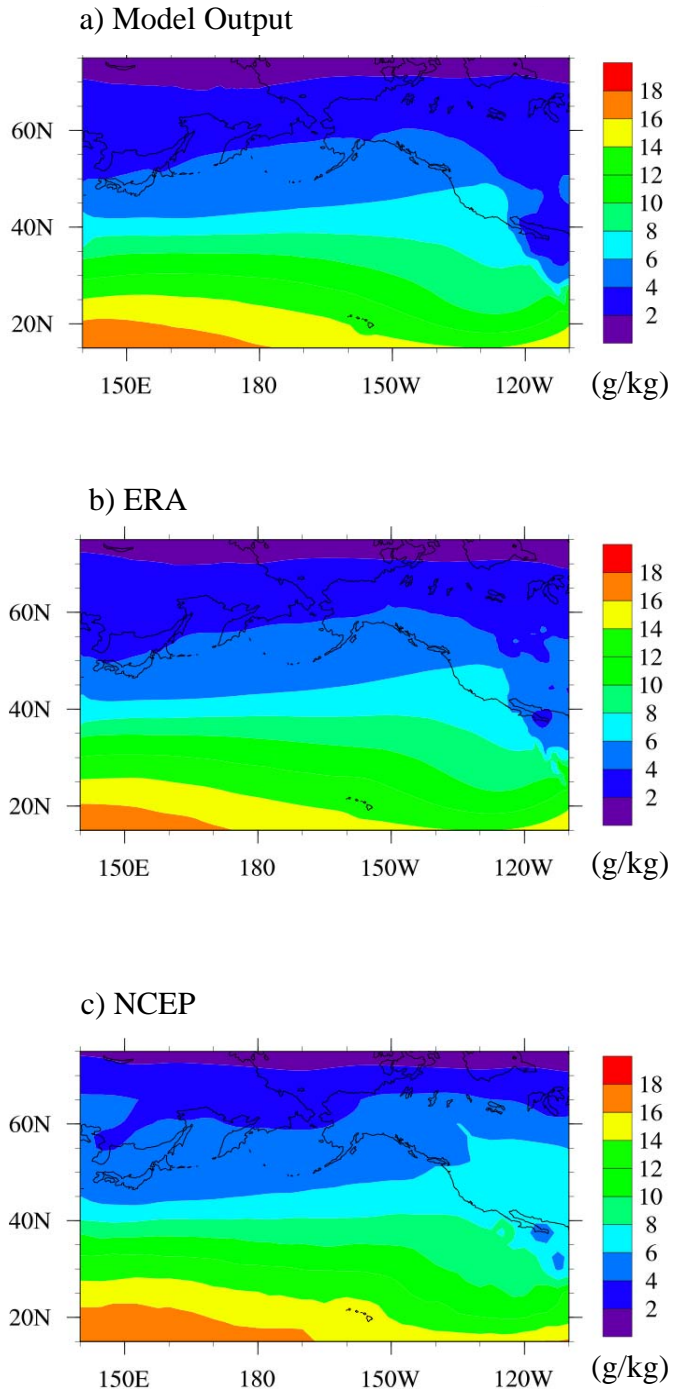


Figure 2.1. Model verification of mean specific humidity. Mean values of specific humidity are shown from January 1981 – December 2001 for (a) model output, (b) ERA, and (c) NCEP.

Sea Level Pressure

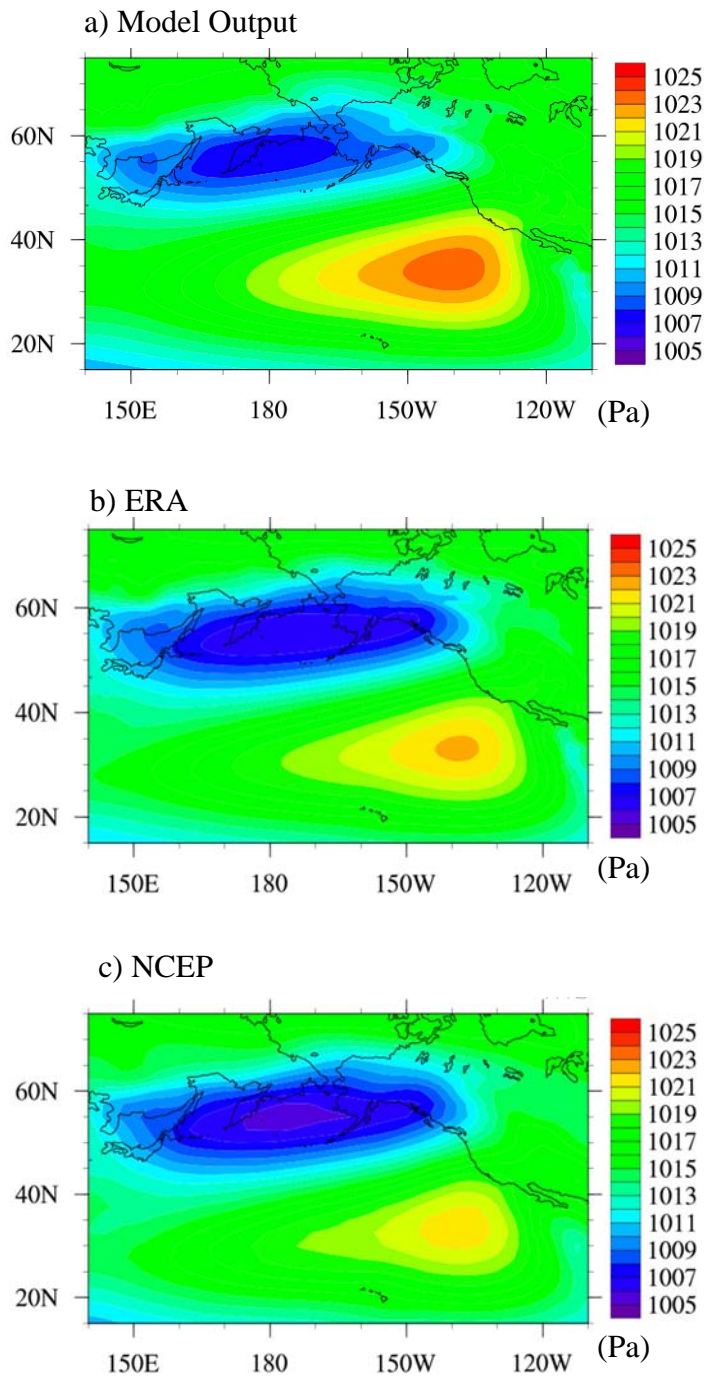


Figure 2.2. Model verification for mean sea level pressure. Mean values of sea level pressure are shown from January 1981 – December 2001 for (a) model output, (b) ERA, and (c) NCEP.

Geopotential Height at 500mb

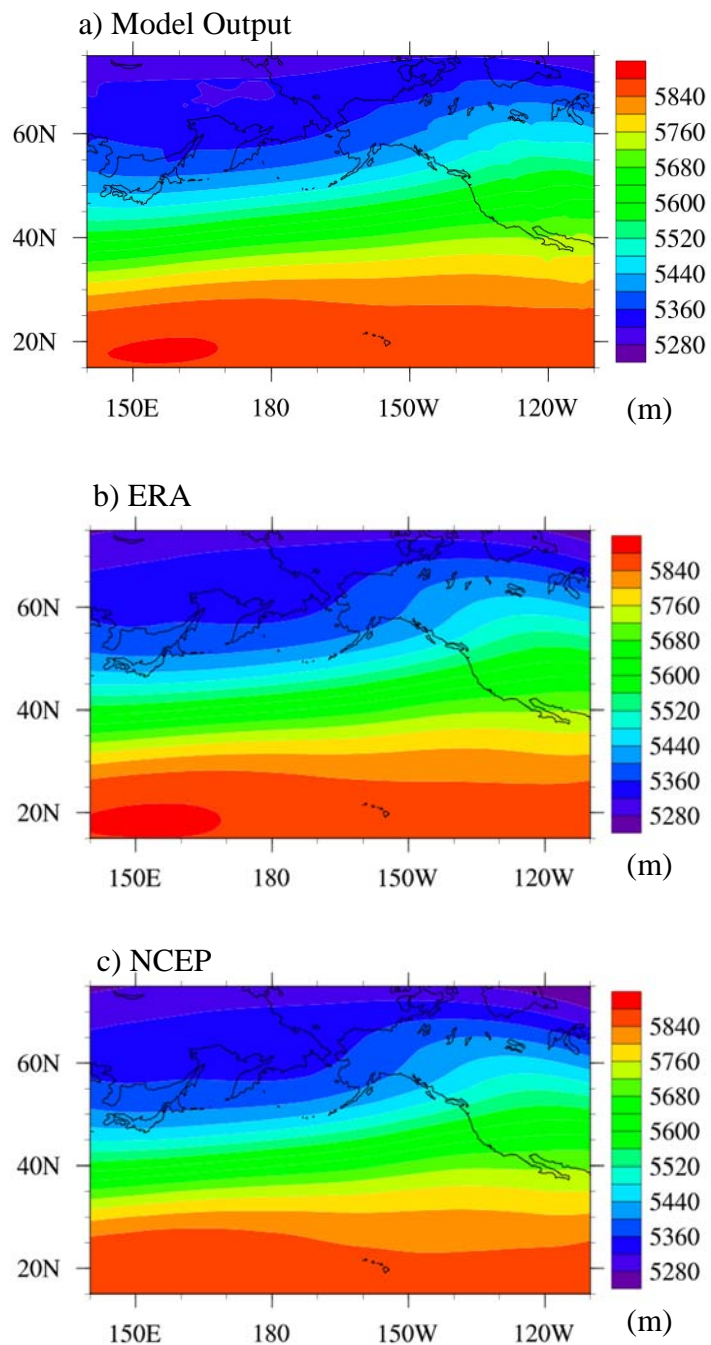


Figure 2.3. Model verification of mean geopotential height at 500mb. Mean values of geopotential height at 500mb are shown from January 1981 – December 2001 for (a) model output, (b) ERA, and (c) NCEP.

Wind Vectors at 850mb

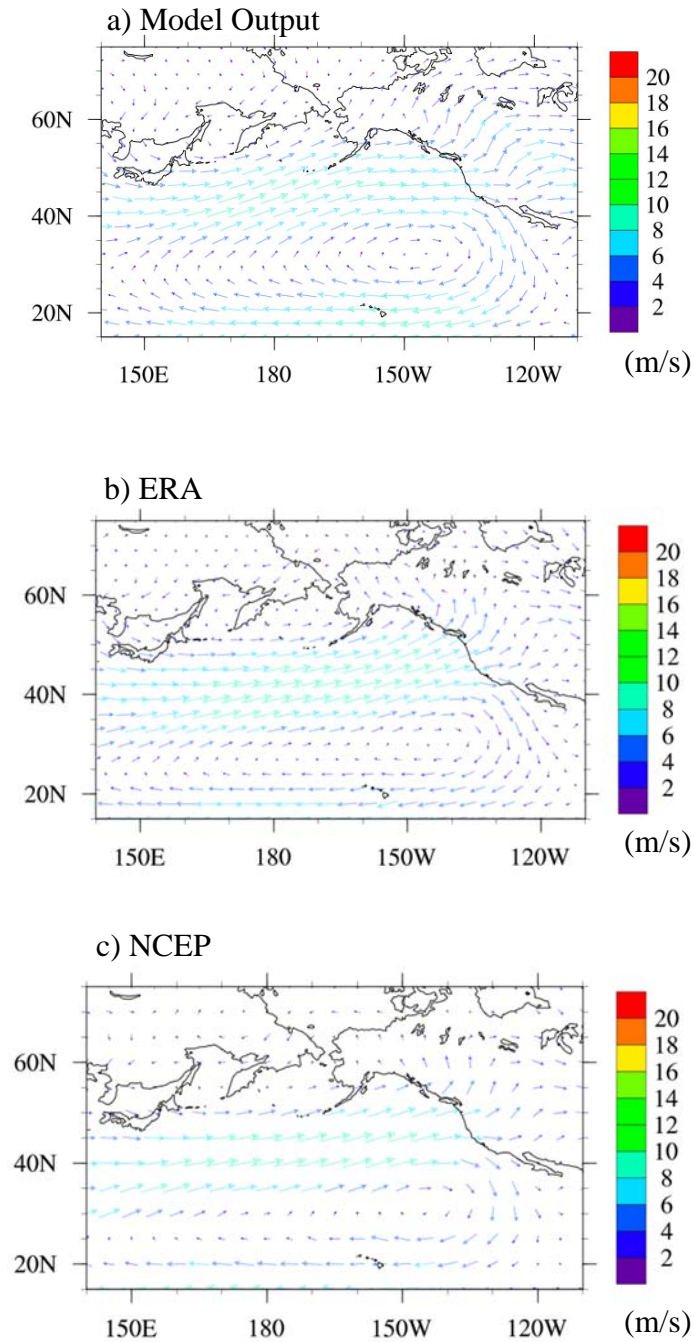


Figure 2.4. Model verification for mean wind at 850mb. Mean values of wind at 850mb are shown from January 1981 – December 2001 for (a) model output, (b) ERA, and (c) NCEP.

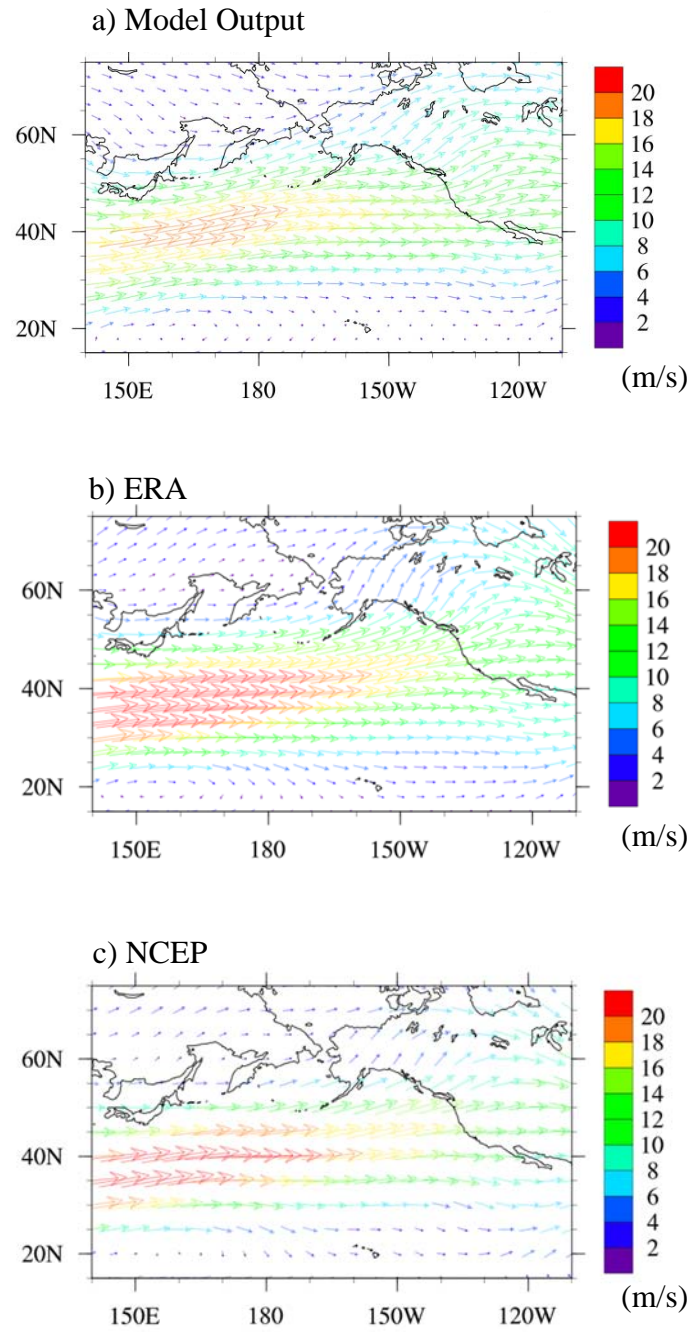


Figure 2.5. Model verification for mean wind at 500mb. Mean values of wind at 500mb are shown from January 1981 – December 2001 for (a) model output, (b) ERA, and (c) NCEP.

2.3 PDO Experiment

A set of sensitivity experiments was conducted to investigate the impacts of the PDO phases on moisture transport into Alaska. In this experiment, SST and sea ice concentration were allowed to vary with time between 10° N to 75° N and 150° E to 140° W (the area of the North Pacific). Elsewhere, both variables were set to their climatological values. The difference between average cool phase SST's and average warm phase SST's is shown in Figure 2.6. After a one-year spin up, the model runs were made from 1945-2002, which includes one cool phase PDO of 31 years (1945-1976) and one warm phase PDO of 25 years (1977-2002). Six-hourly instantaneous outputs from the model runs were obtained. Calculations were made on the six-hourly output, and then seasonal or annual averages were taken. For robustness of the results, this experiment was conducted three times using three different sets of initial conditions.

2.4 PDO and ENSO Experiment

A second set of experiments was conducted in order to examine the impact of interannual SST variability due to global variability with a focus on El Niño and La Niña events. In this experiment, SSTs and sea ice concentrations at all latitudes and longitudes were allowed to vary with time. Three sets of model runs were made from 1945-2002 with different initial conditions, and six-hourly outputs were obtained. Again, calculations were made on the six-hourly output, and then annual or seasonal averages were taken.

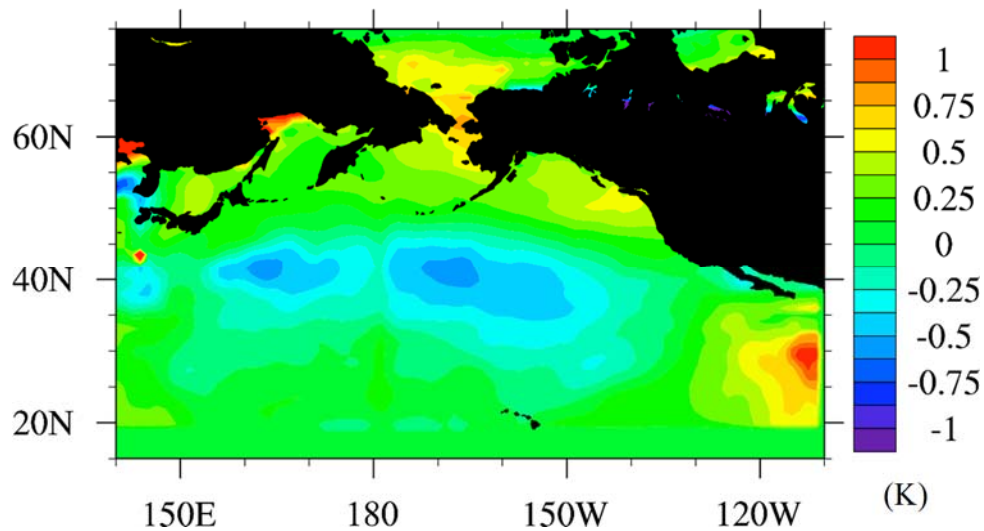


Figure 2.6. SST forcing for CAM5. Warm phase SST minus cool phase SST is shown by color contours for the area of the North Pacific Ocean.

2.5 Data

PDO index data from the Joint Institute for the Study of the Atmosphere and Ocean (JISAO) at the University of Washington was used to determine the years which comprise the cool (December 1945-November 1976) and warm (December 1976-November 2002) PDO phases.

The Niño3.4 index, version ERSST.V3B from the National Weather Service Climate Prediction Center (<http://www.cpc.ncep.noaa.gov/data/indices/3mth.Niño34.81-10.ascii.txt>), was used to determine the periods of El Niño and La Niña events. The data spans 1950-2002 and has a base climatology period from 1981-2010 used to calculate the anomalies.

Chapter 3. Results of the PDO Sensitivity Experiment

3.1 Precipitation

The climate of Alaska is very diverse and comprises of several climate regions. As such, to study the effects of PDO phase on precipitation, the state was separated into five areas to look at these climate regions individually: Barrow (arctic); Fairbanks, Nome, and Anchorage (sub-arctic); and Juneau (continental). Hawaii also has different climate regions due to orographic effects and the trade winds. Two stations on separate islands – Hilo (Hawaii) and Honolulu (Oahu) – were chosen based on their geographic locations and different climates.

Figures 3.1 – 3.4 show the seasonal accumulated precipitation obtained from the National Climate Data Center (NCDC) station data for the period of 1949-2002 in those five areas of Alaska and two areas in Hawaii with a six month running average weight. Seasonal averages of accumulated precipitation are shown in Tables 3.1 – 3.4. Annual accumulated precipitation during warm phase PDO and cool phase PDO is given in Table 3.5. As seen in Table 3.5, station data in Alaska show an increase in mean accumulated precipitation during warm phase PDO. Juneau receives the greatest amounts of precipitation in Alaska with an average accumulation amount of approximately 1,350mm ($\sigma = 195.8\text{mm}$) in cool phase and 1,520mm ($\sigma = 294.8\text{mm}$) in warm phase. Next is Anchorage with approximately 370mm ($\sigma = 68.4\text{mm}$) of precipitation in cool phase and 420mm ($\sigma = 91.9\text{mm}$) in warm phase and Nome with 380mm ($\sigma = 112.2\text{mm}$) of precipitation in cool phase and 440mm ($\sigma = 95.0\text{mm}$) in warm phase. Interior and arctic Alaska receive the least amounts of precipitation. Fairbanks has an annual mean of

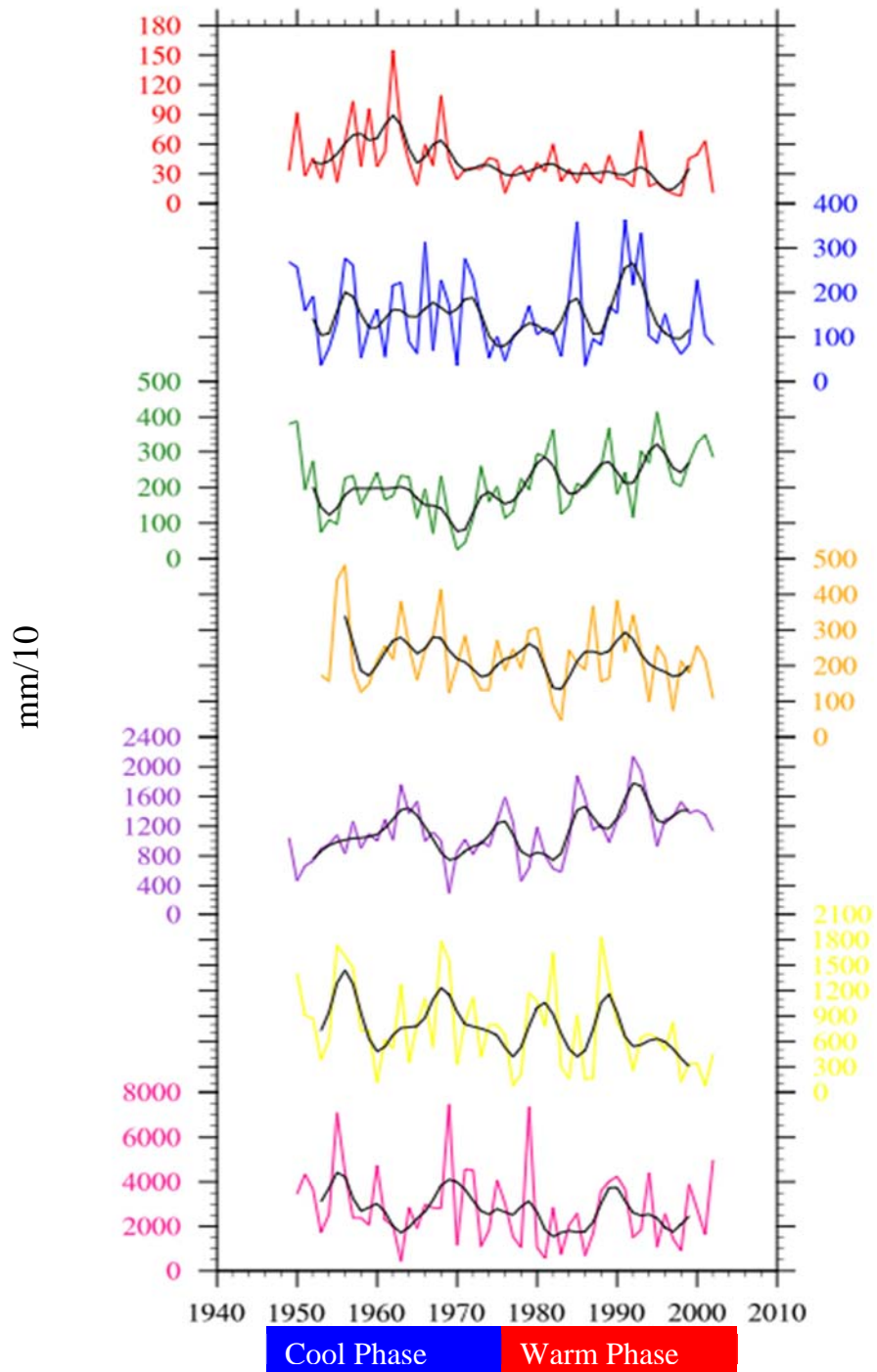


Figure 3.1. Winter accumulated precipitation. Observed winter accumulated precipitation from 1949-2002 is shown for Barrow (red), Fairbanks (blue), Anchorage (green), Nome (orange), Juneau (purple), Honolulu (yellow), and Hilo (pink). A weighted average is applied for each time series (black).

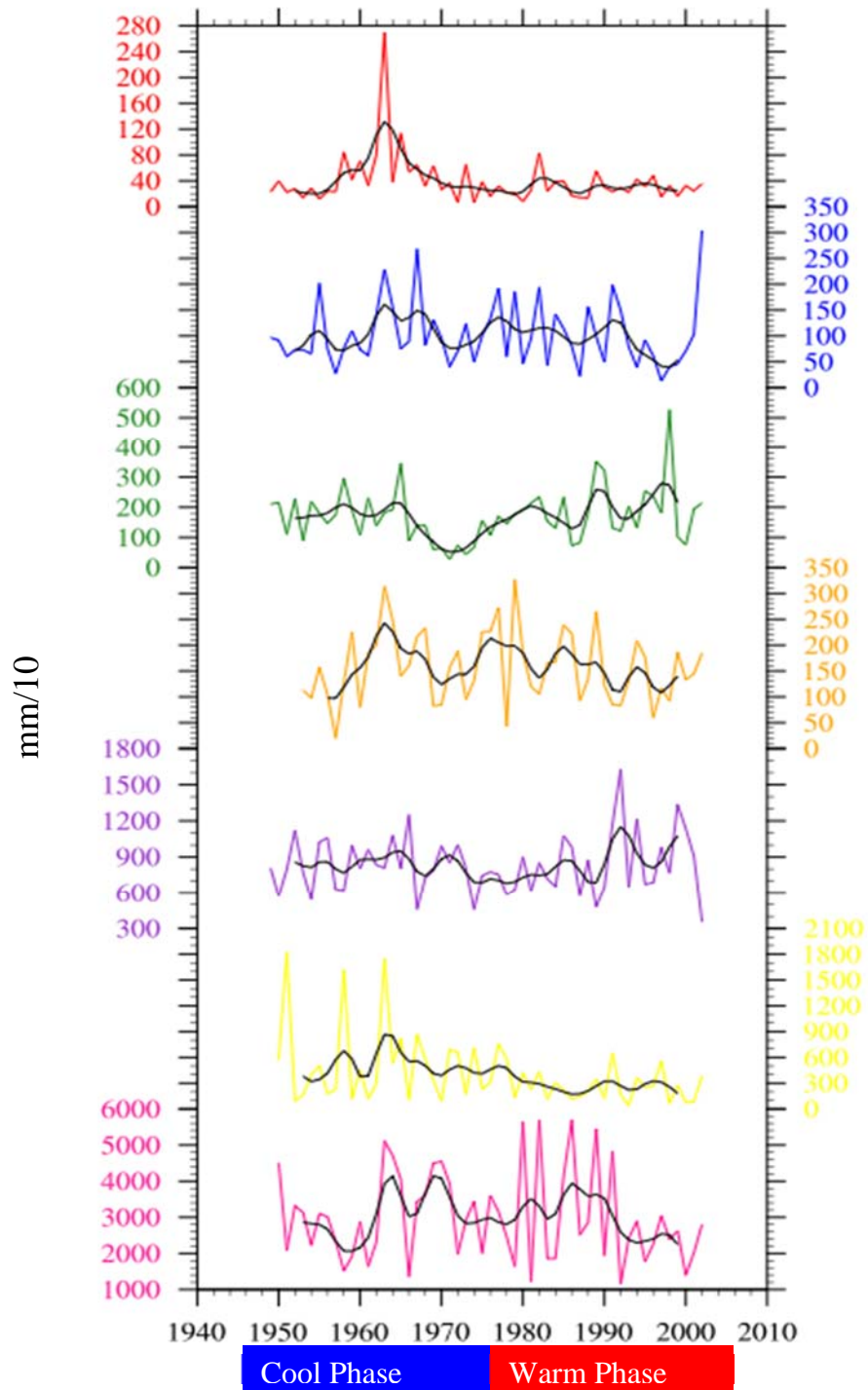


Figure 3.2. Spring accumulated precipitation. Observed spring accumulated precipitation from 1949-2002 is shown for Barrow (red), Fairbanks (blue), Anchorage (green), Nome (orange), Juneau (purple), Honolulu (yellow), and Hilo (pink). A weighted average is applied for each time series (black).

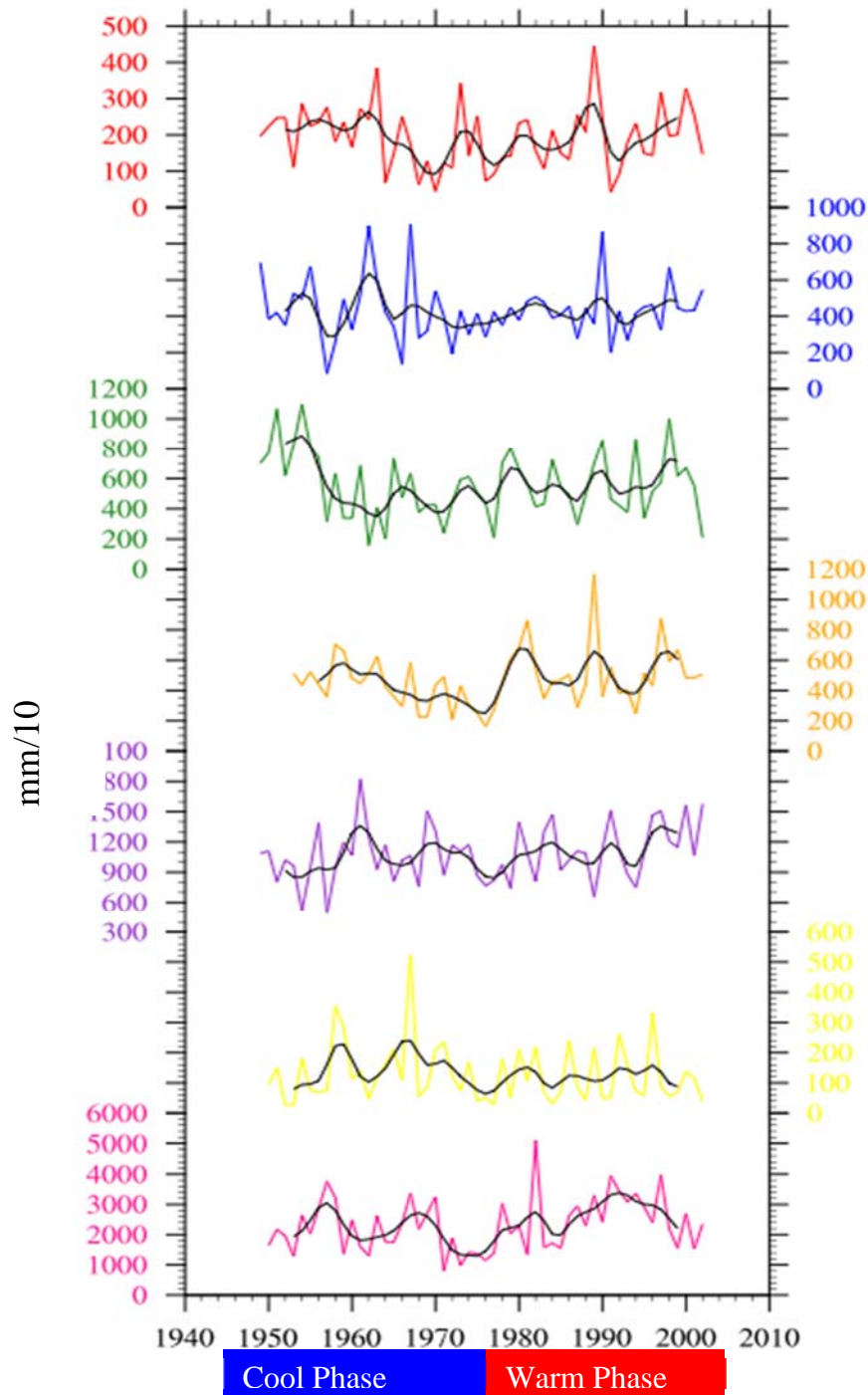


Figure 3.3. Summer accumulated precipitation. Observed summer accumulated precipitation from 1949-2002 is shown for Barrow (red), Fairbanks (blue), Anchorage (green), Nome (orange), Juneau (purple), Honolulu (yellow), and Hilo (pink). A weighted average is applied for each time series (black).

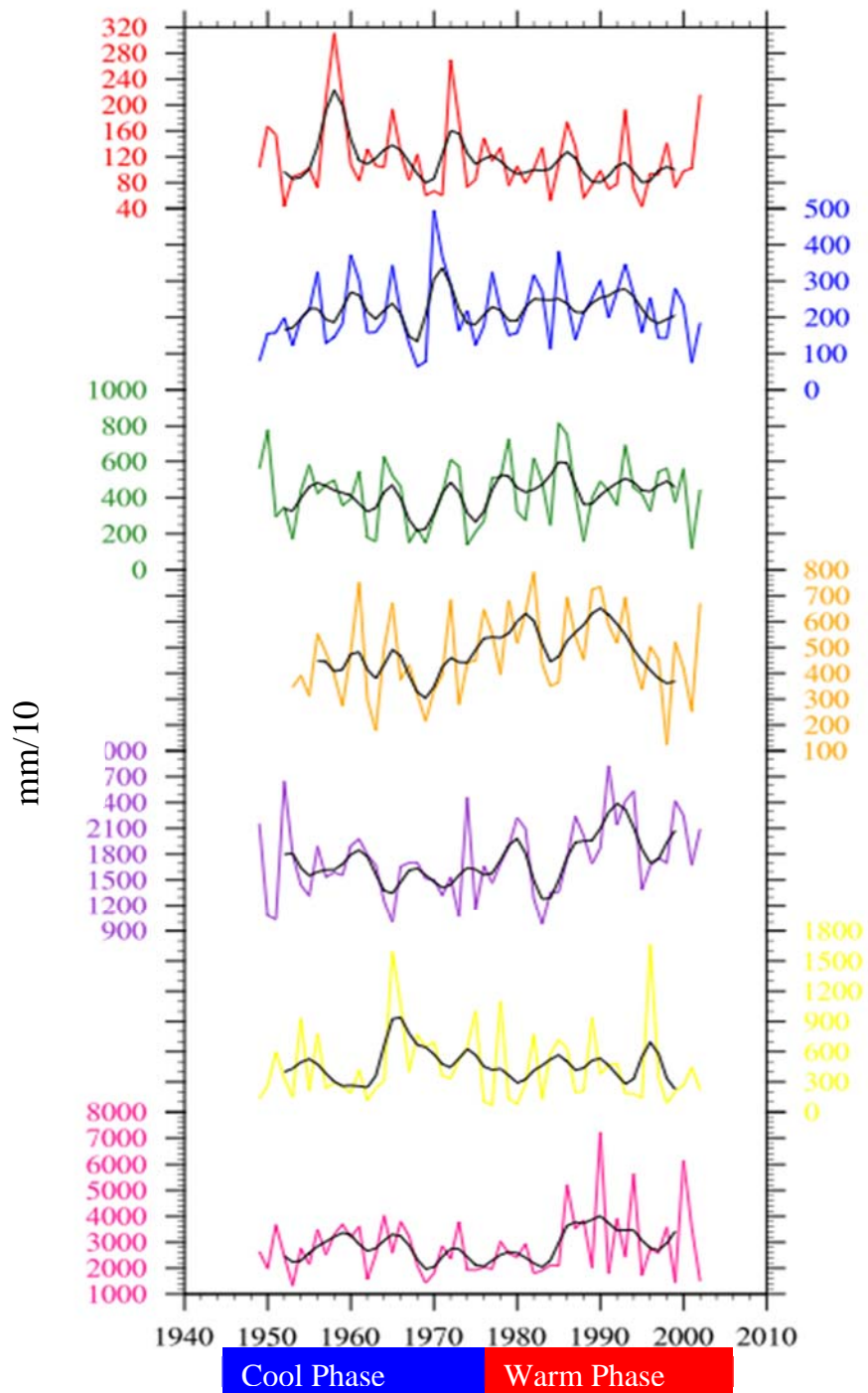


Figure 3.4. Fall accumulated precipitation. Observed fall accumulated precipitation from 1949-2002 is shown for Barrow (red), Fairbanks (blue), Anchorage (green), Nome (orange), Juneau (purple), Honolulu (yellow), and Hilo (pink). A weighted average is applied for each time series (black).

Table 3.1. Mean observed winter accumulated precipitation during warm phase PDO and cool phase PDO.

Observed Winter Mean Precipitation (mm)				
Location	Cool Phase PDO	Cool Phase PDO	Warm Phase PDO	Warm Phase PDO
Barrow	15.6	$\sigma = 9.9$	94.7	$\sigma = 5.2$
Fairbanks	46.2	$\sigma = 26.5$	43.5	$\sigma = 26.9$
Anchorage	69.1	$\sigma = 32.5$	63.9	$\sigma = 25.9$
Nome	53.7	$\sigma = 26.7$	75.0	$\sigma = 23.6$
Juneau	308.6	$\sigma = 93.9$	368.9	$\sigma = 124.1$
Honolulu	258.6	$\sigma = 143.1$	186.4	$\sigma = 144.0$
Hilo	940.4	$\sigma = 494.4$	745.7	$\sigma = 491.9$

Table 3.2. Mean observed spring accumulated precipitation during warm phase PDO and cool phase PDO.

Observed Spring Mean Precipitation (mm)				
Location	Cool Phase PDO	Cool Phase PDO	Warm Phase PDO	Warm Phase PDO
Barrow	14.5	$\sigma = 15.1$	9.0	$\sigma = 4.7$
Fairbanks	30.8	$\sigma = 16.7$	30.9	$\sigma = 20.8$
Anchorage	47.6	$\sigma = 20.7$	46.9	$\sigma = 20.9$
Nome	44.6	$\sigma = 22.7$	58.0	$\sigma = 29.0$
Juneau	166.2	$\sigma = 40.7$	161.8	$\sigma = 67.7$
Honolulu	160.1	$\sigma = 147.4$	84.4	$\sigma = 57.9$
Hilo	924.1	$\sigma = 320.8$	874.2	$\sigma = 429.6$

Table 3.3. Mean observed summer accumulated precipitation during warm phase PDO and cool phase PDO.

Observed Summer Mean Precipitation (mm)				
Location	Cool Phase PDO	Cool Phase PDO	Warm Phase PDO	Warm Phase PDO
Barrow	58.4	$\sigma = 25.8$	58.2	$\sigma = 25.7$
Fairbanks	129.5	$\sigma = 58.6$	130.8	$\sigma = 38.1$
Anchorage	126.1	$\sigma = 44.2$	157.0	$\sigma = 60.9$
Nome	167.3	$\sigma = 71.1$	167.4	$\sigma = 60.2$
Juneau	312.0	$\sigma = 83.6$	339.3	$\sigma = 82.4$
Honolulu	42.2	$\sigma = 33.3$	35.0	$\sigma = 25.1$
Hilo	622.3	$\sigma = 236.0$	773.4	$\sigma = 276.6$

Table 3.4. Mean observed fall accumulated precipitation during warm phase PDO and cool phase PDO.

Observed Fall Mean Precipitation (mm)				
Location	Cool Phase PDO	Cool Phase PDO	Warm Phase PDO	Warm Phase PDO
Barrow	38.1	$\sigma = 19.5$	31.4	$\sigma = 12.7$
Fairbanks	61.6	$\sigma = 30.7$	67.6	$\sigma = 23.1$
Anchorage	127.4	$\sigma = 45.3$	154.7	$\sigma = 48.4$
Nome	116.1	$\sigma = 52.9$	138.7	$\sigma = 52.0$
Juneau	481.1	$\sigma = 120.0$	562.6	$\sigma = 131.8$
Honolulu	145.0	$\sigma = 106.1$	125.6	$\sigma = 112.3$
Hilo	791.1	$\sigma = 244.3$	919.5	$\sigma = 453.4$

Table 3.5. Mean observed annual accumulated precipitation during warm phase PDO and cool phase PDO.

Observed Annual Mean Precipitation (mm)				
Location	Cool Phase PDO	Cool Phase PDO	Warm Phase PDO	Warm Phase PDO
Barrow	123.1	$\sigma = 51.0$	108.0	$\sigma = 29.2$
Fairbanks	268.1	$\sigma = 71.4$	272.8	$\sigma = 57.1$
Anchorage	370.2	$\sigma = 68.4$	422.5	$\sigma = 91.9$
Nome	378.1	$\sigma = 112.2$	439.1	$\sigma = 95.0$
Juneau	1,349.1	$\sigma = 195.8$	1,522.9	$\sigma = 294.8$
Honolulu	597.9	$\sigma = 266.3$	431.3	$\sigma = 214.8$
Hilo	3,189.1	$\sigma = 805.6$	3,312.8	$\sigma = 884.1$

approximately 270mm ($\sigma = 71.4\text{mm}$ in cool phase and $\sigma = 57.1\text{mm}$ in warm phase) in both PDO phases. Accumulated precipitation in Barrow decreases during warm phase PDO from an annual mean of 120mm ($\sigma = 51.0\text{mm}$) in the cool phase to 100mm ($\sigma = 29.2\text{mm}$). Station data from Hawaii show both a decrease and an increase in accumulated precipitation during warm phase PDO. Hilo, located on the east side of Hawaii, receives an average of approximately 3,200mm ($\sigma = 805.6\text{mm}$) in precipitation during the cool phase and 3,300mm ($\sigma = 884.1\text{mm}$) during the warm phase. Honolulu is located on the south side of Oahu and receives much less precipitation: 600mm ($\sigma = \text{mm}$) in cool phase and 430mm ($\sigma = 214.8\text{mm}$) in the warm phase.

These results are compared to changes in seasonal accumulated precipitation from CAM5 output shown in Figure 3.5. In Figure 3.5a, the model shows increases in wintertime precipitation at all stations during warm phase PDO. In spring (Figure 3.5b), model output shows increases in seasonal precipitation during warm phase PDO throughout most of Alaska except Juneau and decreases in both locations in Hawaii. Summertime precipitation (Figure 3.5c) increases in arctic Alaska and Hawaii but decreases in the remaining stations in Alaska. Precipitation in fall also increases at all stations during warm phase PDO (Figure 3.5d).

The differences between model output and station data can be explained. Monitoring of precipitation over the past 60 years has not been consistent, especially in Alaska, resulting in missing climate data. Furthermore, while measurement methods have become more accurate, the data is still skewed as they represent point sources.

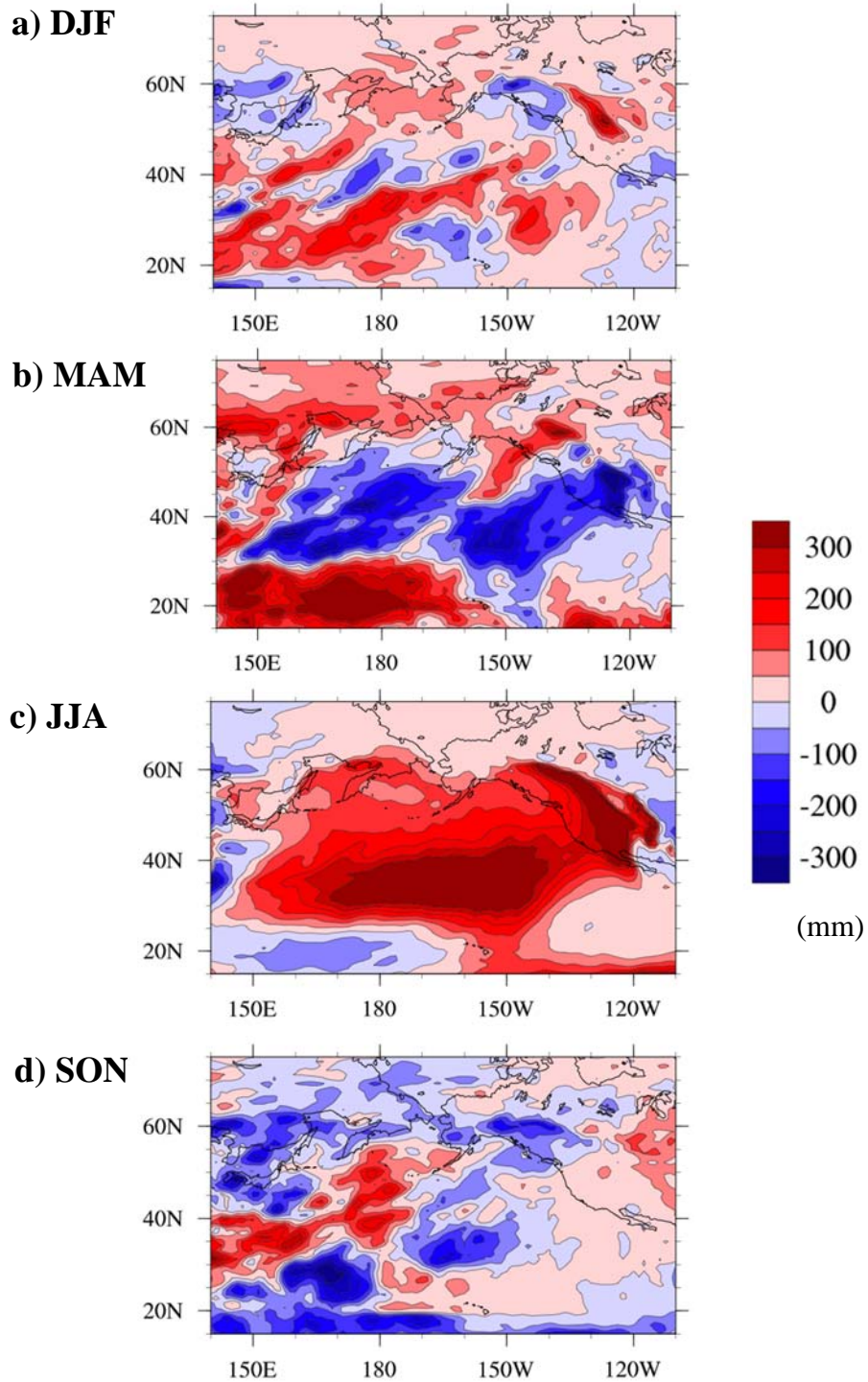


Figure 3.5. PDO difference of accumulated precipitation. The difference between warm phase and cool phase (warm – cool) PDO seasonal accumulated precipitation is shown for a) DJF, b) MAM, c) JJA, and d) SON.

3.2 Moisture Convergence

For a better understanding of changes in precipitation, we examine the changes in the amount of moisture coming into an area, defined as moisture convergence (MC), which is determined by:

$$MC = -\nabla \cdot (q\mathbf{v})$$

$$MC = -\left(\frac{\partial(qu)}{\partial x} + \frac{\partial(qv)}{\partial y}\right)$$

Eq. 3.1.

The moisture convergence throughout the atmosphere up to 300mb is calculated by taking the vertical integral of MC with respect to pressure:

$$MC_{total} = \frac{-1}{g} \int_{sfc}^{300mb} \left(\frac{\partial(qu)}{\partial x} + \frac{\partial(qv)}{\partial y}\right) dp$$

Eq. 3.2.

The greatest areas of moisture divergence over the North Pacific occur near the equator, as humid air from the tropics is transported out of the area. Varying amounts of convergence occur throughout the North Pacific with orographic lifting along the Rocky Mountains in the North America being responsible for some of the largest amounts of moisture convergence in the region.

The differences in vertically-integrated moisture convergence between the warm phase and cool phase (warm – cool) PDO are shown in Figure 3.6. In winter (Figure 3.6a) and spring (Figure 3.6b), moisture convergence in Alaska, along the northwestern coast of North America, and Hawaii decreases. Moisture convergence increases over the northwestern United States, throughout western portions of Canada, and over the eastern Aleutian Islands and arctic region of Alaska during summer (Figure 3.6c), but still

decreases in Hawaii and throughout interior Alaska. In fall (Figure 3.6d), a decrease occurs in Alaska, Hawaii, and the northwest United States, and an increase occurs over northwest Canada.

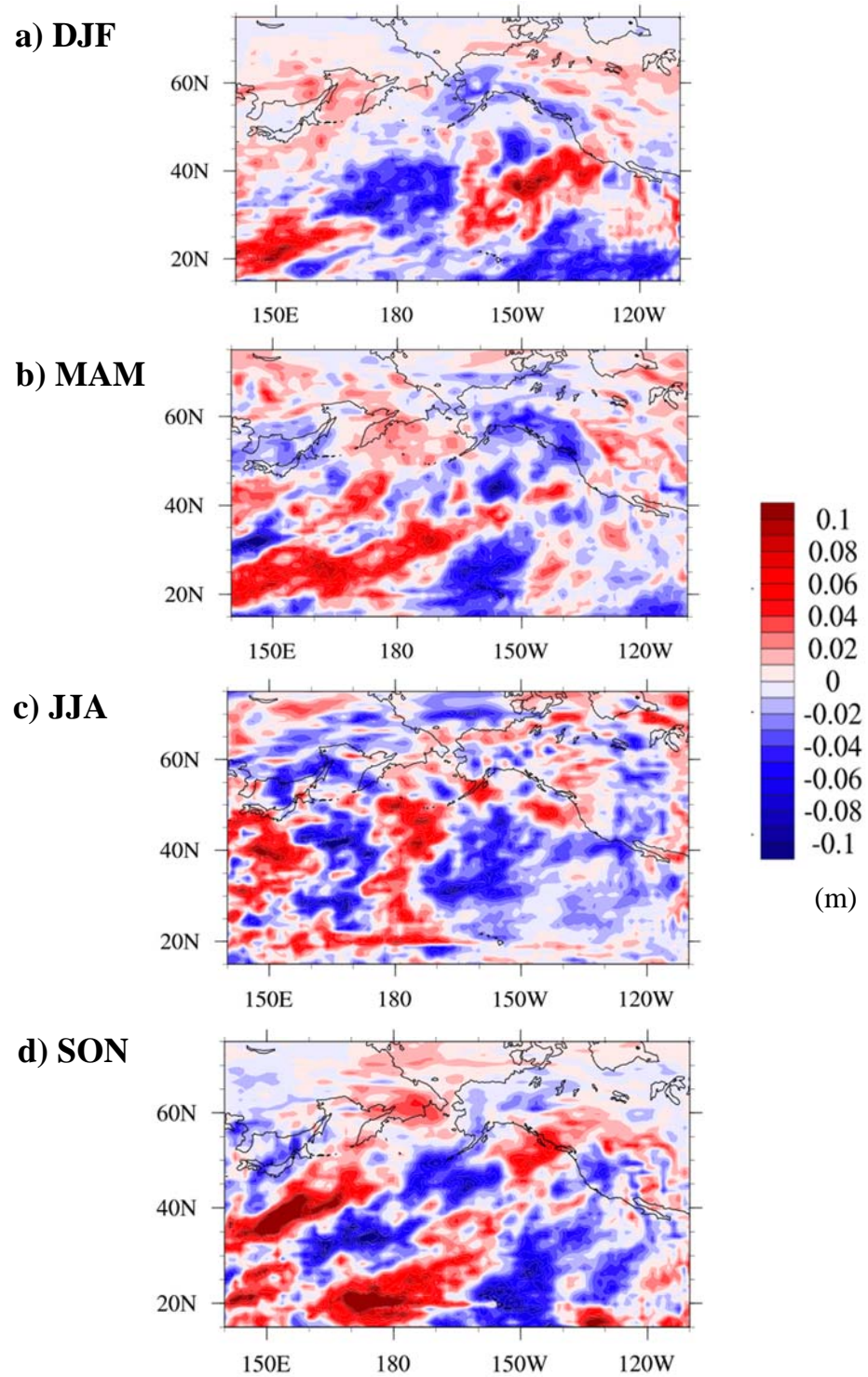


Figure 3.6. PDO difference of moisture convergence. The difference between warm phase and cool phase (warm – cool) PDO vertically-integrated mean seasonal moisture convergence is shown for a) DJF, b) MAM, c) JJA, and d) SON.

3.3 Moisture Transport

The changes in moisture convergence can happen due to changes in moisture transport. The moisture transport is defined as the product of the specific humidity, q , and the wind vector, \mathbf{v} . For the entire atmosphere, the vertically-integrated total moisture transport (MT_{total}) is calculated by:

$$MT_{total} = \frac{1}{g} \int_{sfc}^{300mb} (q\mathbf{v}) dp \quad \text{Eq. 3.3.}$$

Annual means of moisture transport during each PDO phase shows that moisture flows north and east into Alaska and the western coastline of North America but flows west over Hawaii (Figures 3.7a and 3.7b). Changes in total moisture transport over the North Pacific between the warm and cool phases of the PDO are shown in Figure 3.7c. Total moisture transport increases in the warm phase PDO throughout Alaska and the western region of North America. However, transport decreases over Hawaii and the southerly portions of the North Pacific.

By introducing the Reynold's Average of q and \mathbf{v} , the total moisture transport is defined as:

$$q\mathbf{v} = (\bar{q} + q')(\bar{\mathbf{v}} + \mathbf{v}') \quad \text{Eq. 3.4,}$$

where an overbar denotes time mean, and a prime denotes deviations from the time mean.

Expanding this equation gives:

$$q\mathbf{v} = \bar{q}\bar{\mathbf{v}} + \bar{q}\mathbf{v}' + q'\bar{\mathbf{v}} + q'\mathbf{v}' \quad \text{Eq. 3.5.}$$

The first term of Equation 3.5 is just the time-averaged moisture transport. The contributions to the total moisture transport by the second and third terms of Equation 3.5

are shown in Figures 3.8 and 3.9 respectively. As these contributions are much less than the mean moisture transport, they can be ignored. Therefore, changes in moisture transport are explained by the fourth term of Equation 3.5, the transient term, $q'v'$.

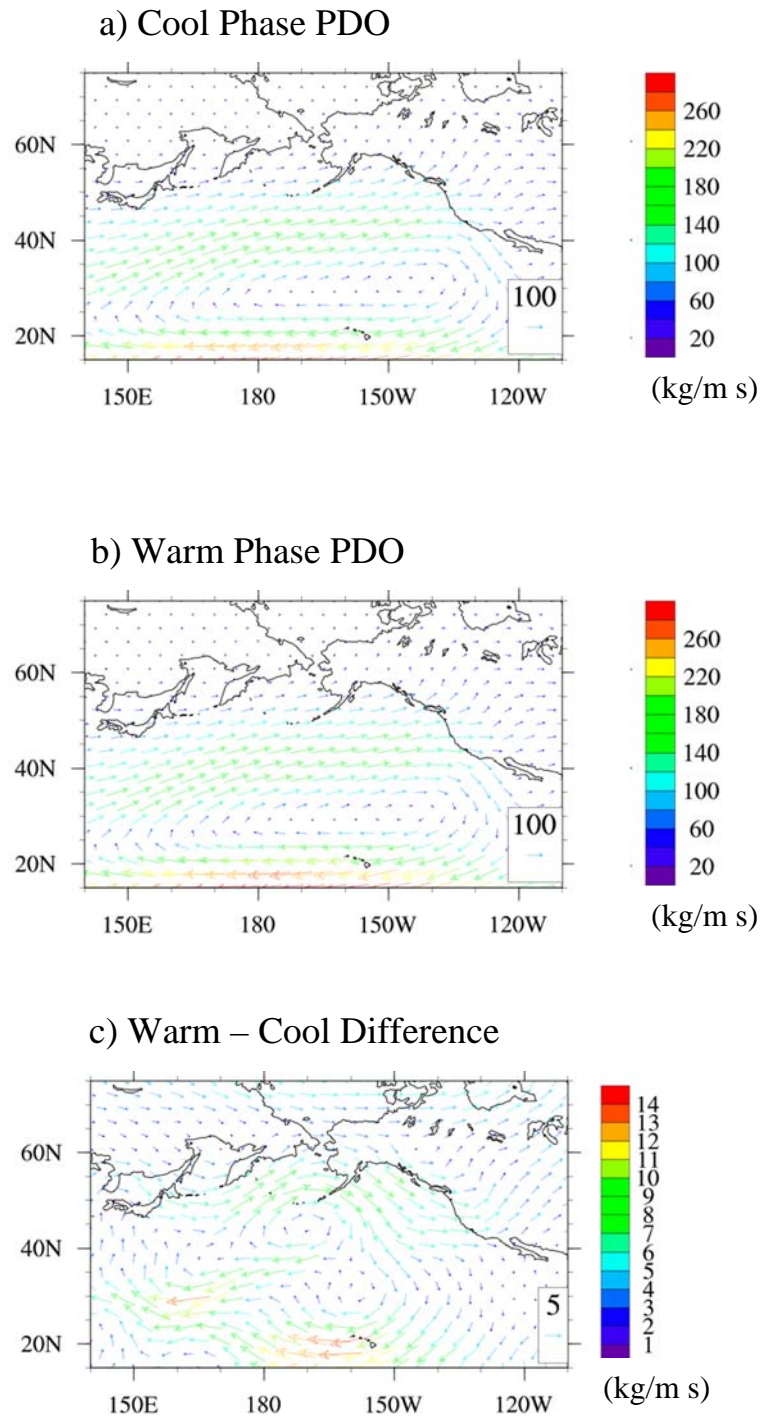


Figure 3.7. PDO difference of mean moisture transport. Annual mean moisture transport is shown during (a) cool phase and (b) warm phase PDO and (c) the difference between phases.

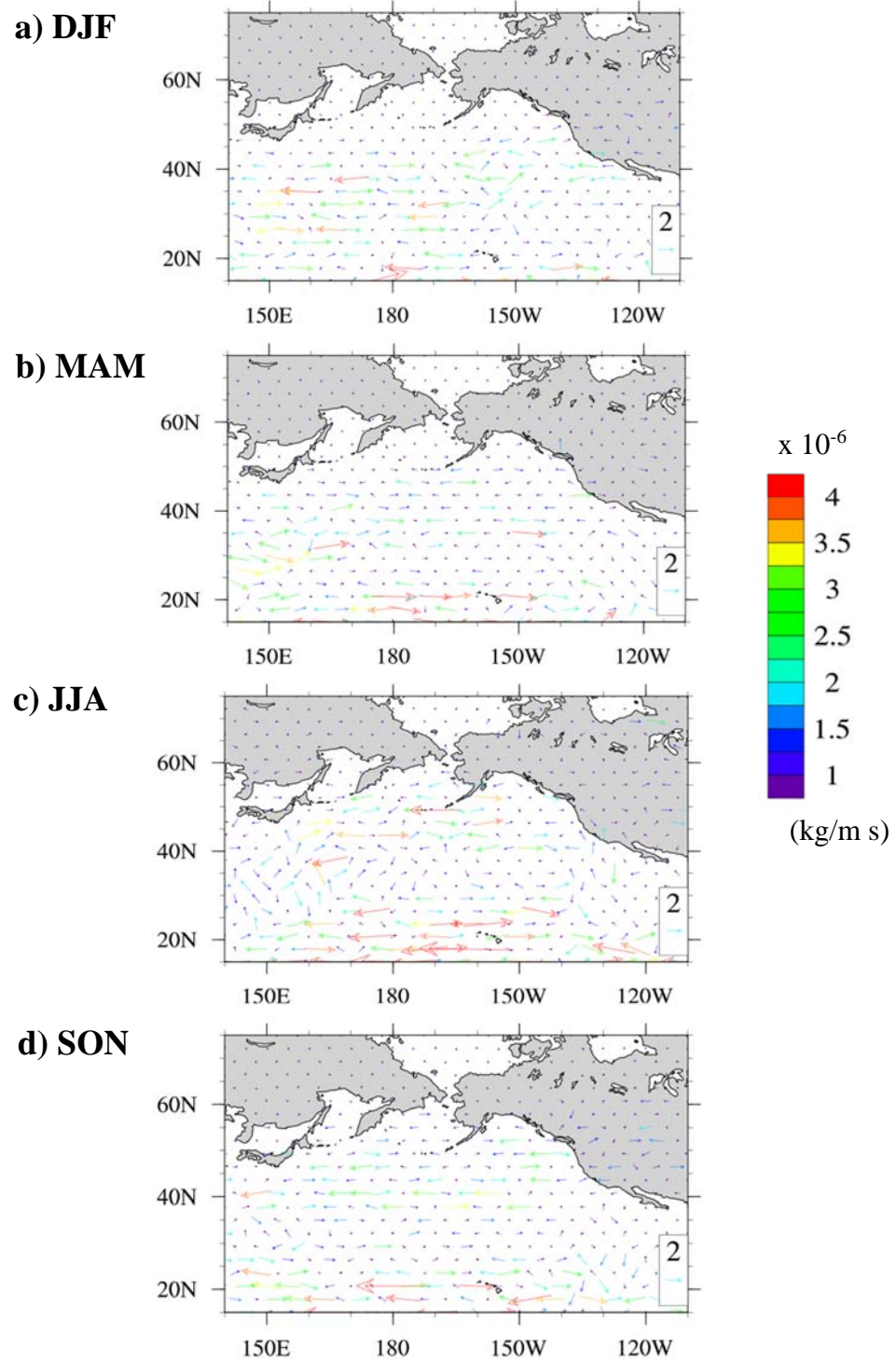


Figure 3.8. PDO difference of term 2 of Equation 3.5. The difference between warm phase and cool phase (warm – cool) PDO vertically-integrated seasonal mean of second term in Equation 3.5 is shown for a) DJF, b) MAM, c) JJA, and d) SON.

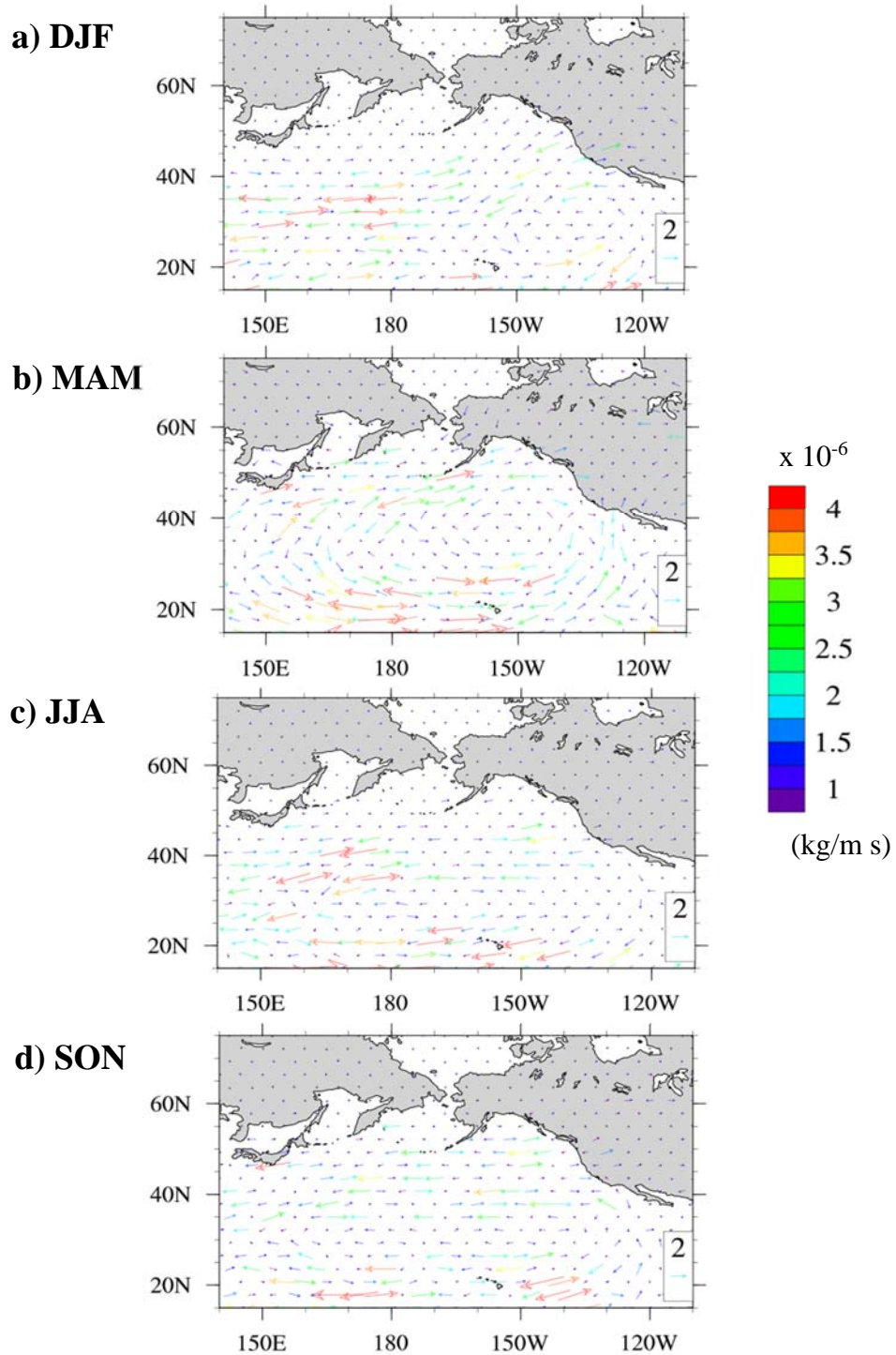


Figure 3.9. PDO difference of term 3 of Equation 3.5. The difference between warm phase and cool phase (warm – cool) PDO vertically-integrated seasonal mean of third term in Equation 3.5 is shown for a) DJF, b) MAM, c) JJA, and d) SON.

Following Zhu and Newell (1998) the vertically-integrated transient moisture transport ($MT_{transient}$) is calculated by:

$$MT_{transient} = \frac{1}{g} \int_{sfc}^{300mb} (q' \mathbf{v}') dp \quad \text{Eq. 3.6.}$$

The differences between warm phase and cool phase transient moisture transport are shown in Figure 3.10. Transient moisture transport into Alaska, along the western coast of the United States, and over Hawaii is greater in the warm phase PDO in winter (Figure 3.10a). For the spring (Figure 3.10b), transient moisture transport decreases in the warm phase over Alaska and throughout much of the North Pacific Ocean but increases over Hawaii. Differences in transient moisture transport show a decrease over the western North Pacific and an increase over the eastern North Pacific during the warm phase PDO in the summer season (Figure 3.10c). In the fall (Figure 3.10d), transient moisture transport increases throughout most of the North Pacific.

To quantify these results, Alaska was enclosed in four boundaries: 1) from 59° N to 70° N along the 165° W longitude, 2) from 165° W to 142° W along the 70° N latitude, 3) from 59° N to 70° N along the 142° W longitude, and 4) from 165° W to 142° W along the 59° N latitude (Figure 3.11), and the net moisture transport across those boundaries was studied. The moisture transport along each boundary was calculated and summed to determine how much the moisture transport fluctuates during PDO phase changes. Positive values indicate that more moisture is entering the area or crossing the boundary than leaving and vice versa. The time series of seasonal net moisture transport into Alaska (the sum of all four boundaries) is shown in Figure 3.12.

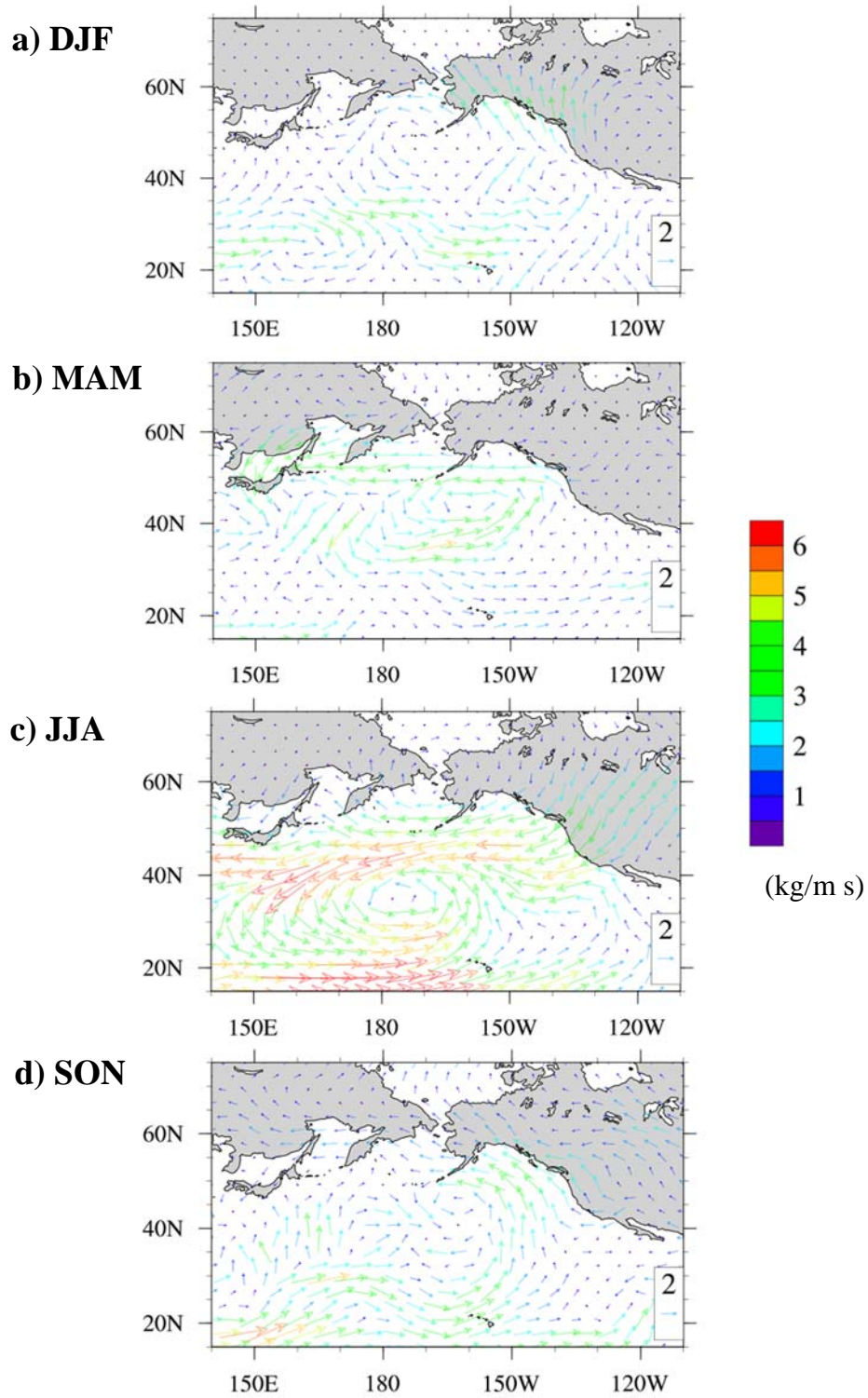


Figure 3.10. PDO difference of transient moisture transport. The mean seasonal transient moisture transport differences between warm and cool phase PDO are shown for a) DJF, b) MAM, c) JJA, and d) SON.

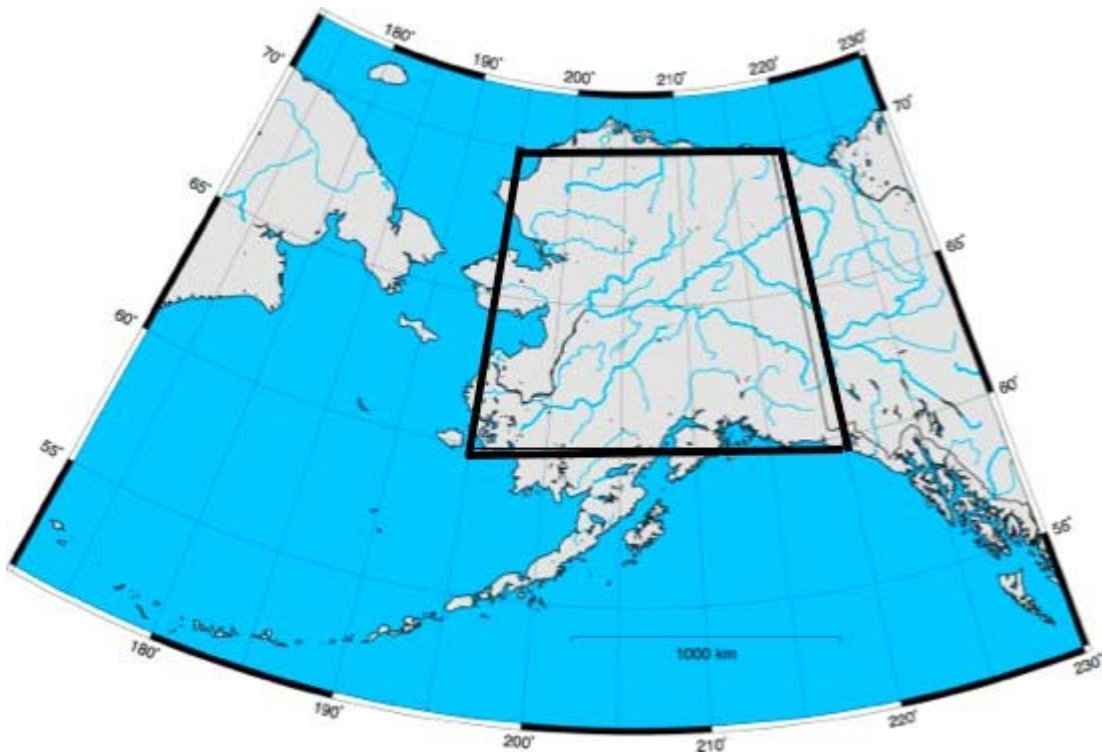


Figure 3.11. Boundaries for net transport calculation. The approximate boundaries for the calculation of net moisture transport into Alaska are shown by the black grid over Alaska. Figure credit: www.geospatialdesktop.com

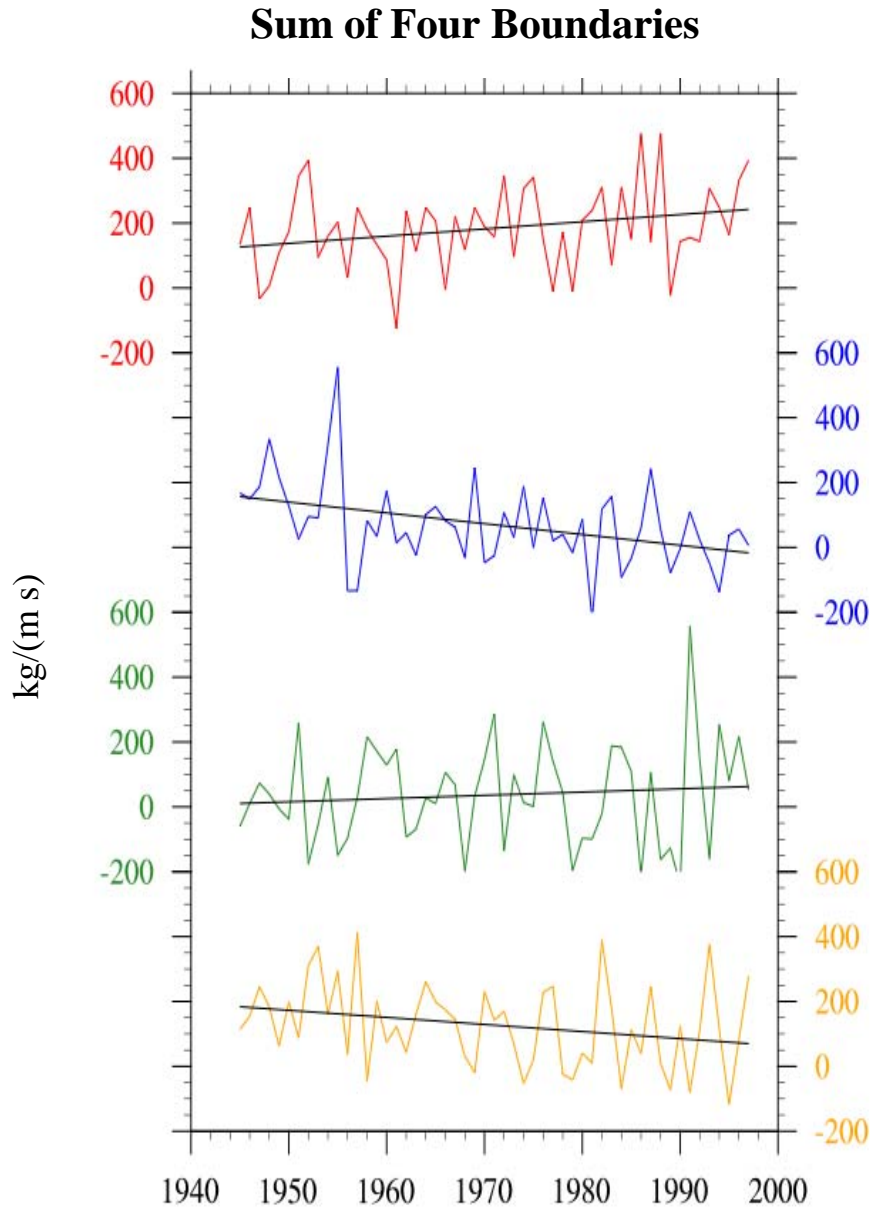


Figure 3.12. Seasonal net transport into Alaska. The time series of seasonal net moisture transport into Alaska is shown for DJF (red), MAM (blue), JJA (green), and SON (orange) and seasonal trend (black).

Net moisture transport into Alaska increases from an average of 170 kg/(m s) in cool phase PDO to 200 kg/(m s) in warm phase PDO in winter. Decreases are seen in spring (from 100 kg/(m s) in cool phase to 20 kg/(m s) in warm phase) and fall (from 150 kg/(m s) in cool phase to 90 kg/(m s) in warm phase). Net moisture transport in summer is similar in both PDO phases at about 35 kg/(m s).

These changes in net moisture transport can be further investigated by looking at the fluctuations along the individual boundaries. Moisture transport along boundary 1 is on average positive for all seasons except spring and increases during warm phase PDO occur in all seasons except winter (Figure 3.13). Moisture transport across boundaries 2 (Figure 3.14) and 3 (Figure 3.15) is negative during both PDO phases meaning that more moisture is leaving Alaska along these north and east boundaries than entering. During warm phase PDO, the amount of moisture crossing these boundaries decreases in most seasons or remains nearly constant. The greatest amounts of moisture entering Alaska occur along the southern boundary (Figure 3.16). As the PDO phase changes, moisture transport along this southern boundary increases in winter and summer and decreases in spring and fall, similar to the changes in net moisture transport into Alaska.

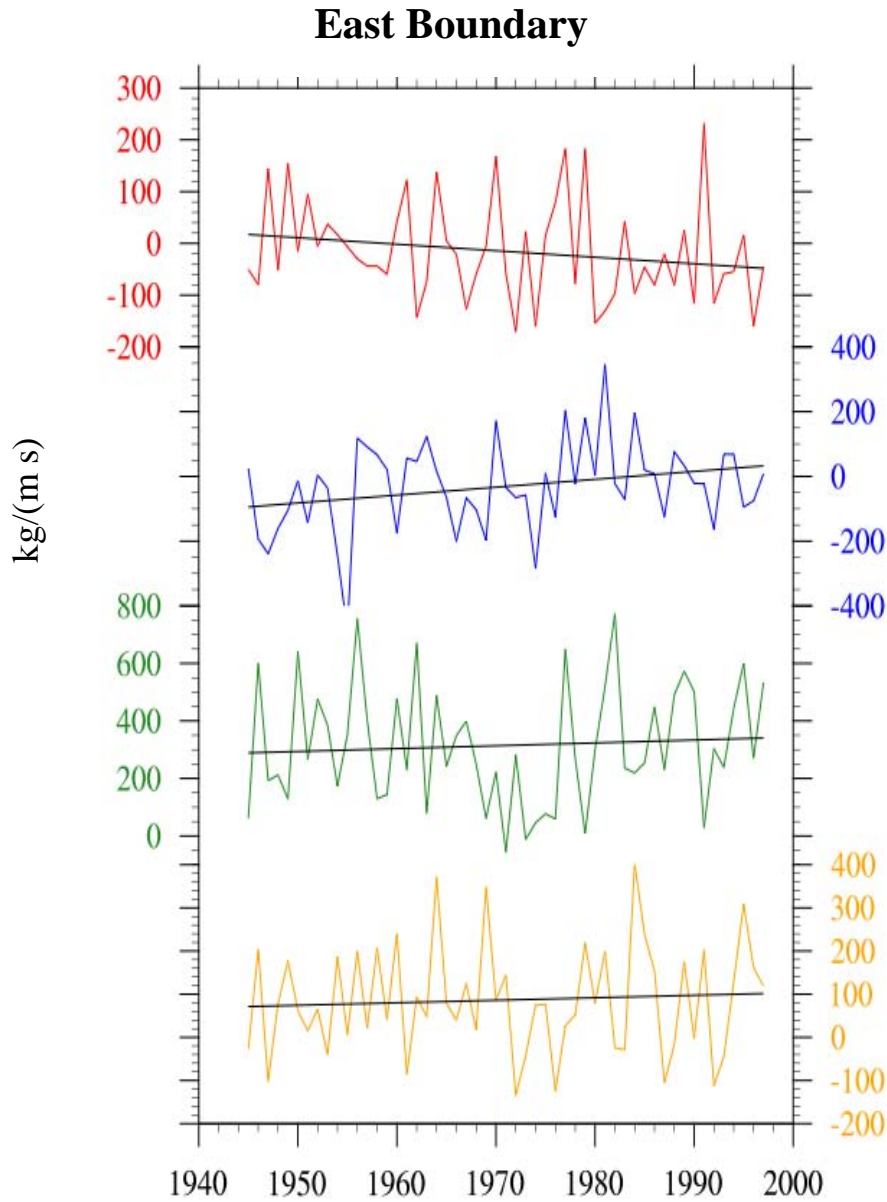


Figure 3.13. Seasonal net transport across east boundary. The time series of seasonal moisture transport across the eastern boundary of Alaska is shown for DJF (red), MAM (blue), JJA (green), and SON (orange) and seasonal trend (black).

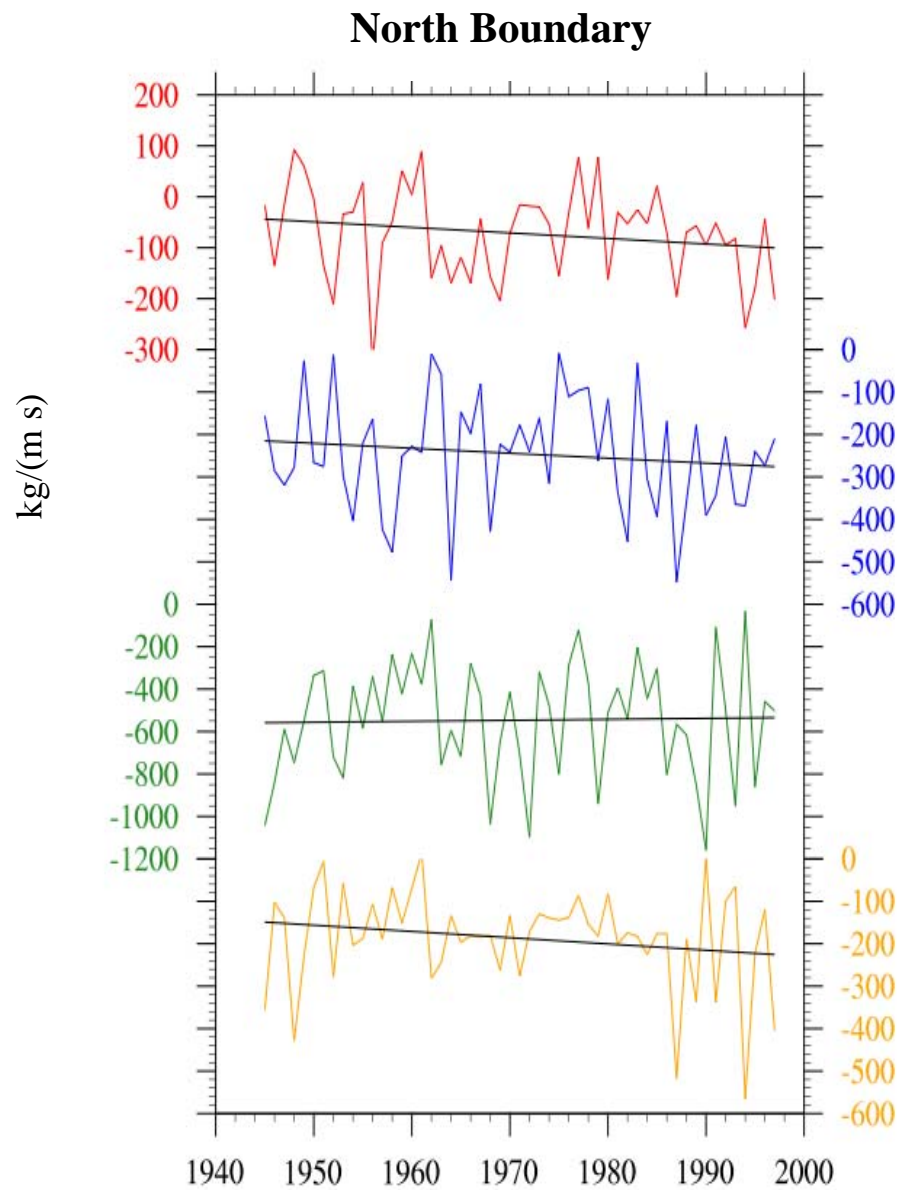


Figure 3.14. Seasonal net transport across north boundary. The time series of seasonal moisture transport across the northern boundary of Alaska is shown for DJF (red), MAM (blue), JJA (green), and SON (orange) and seasonal trend (black).

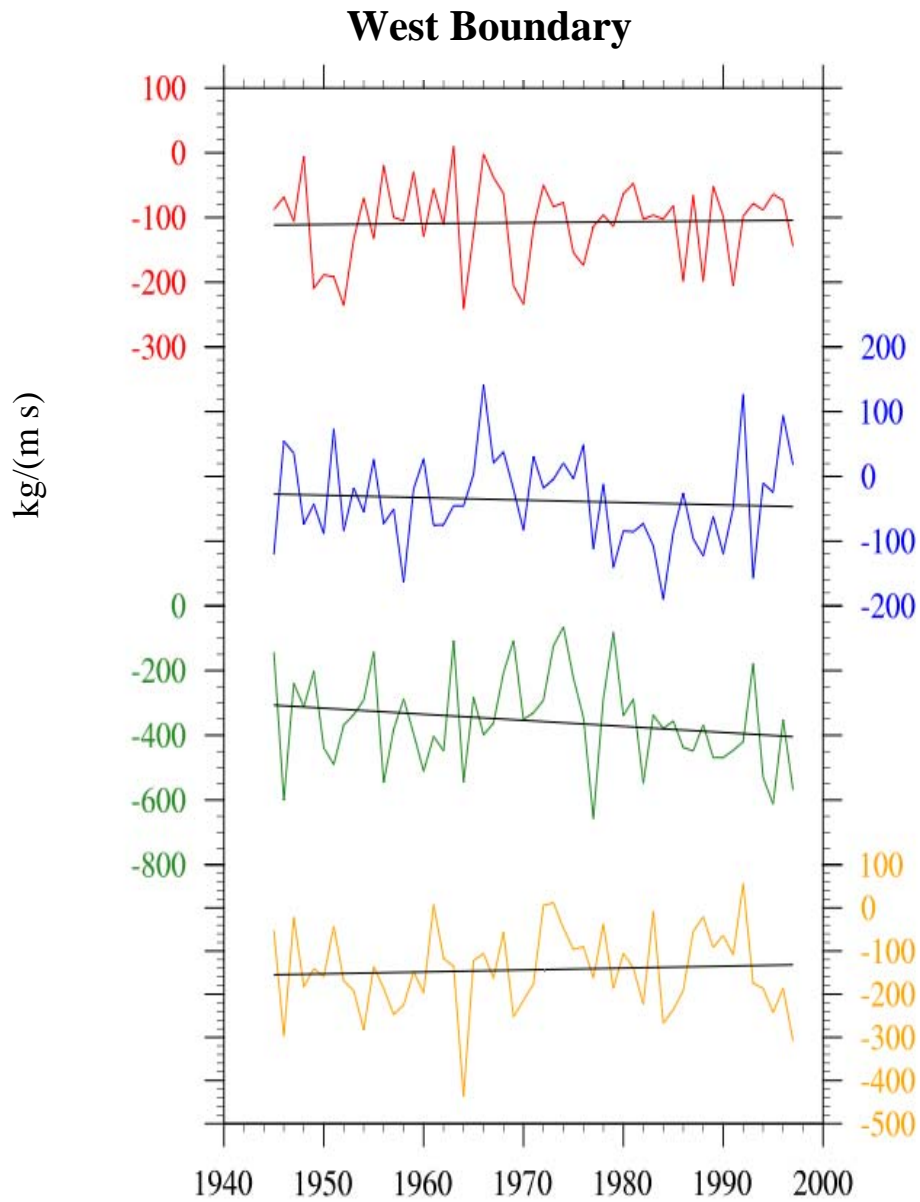


Figure 3.15. Seasonal net transport across west boundary. The time series of seasonal moisture transport across the western boundary of Alaska is shown for DJF (red), MAM (blue), JJA (green), and SON (orange) and seasonal trend (black).

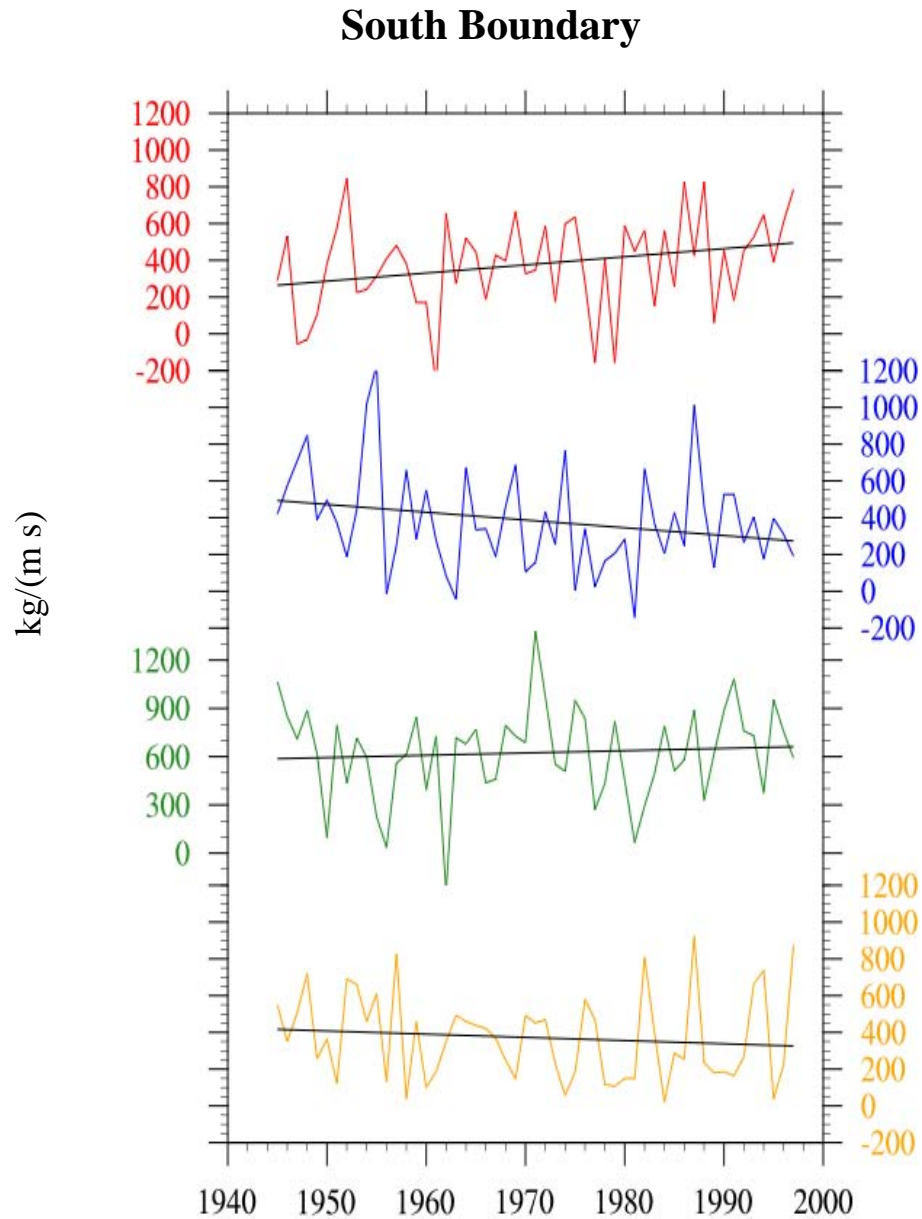


Figure 3.16. Seasonal net transport across south boundary. The time series of seasonal moisture transport across the southern boundary of Alaska is shown for DJF (red), MAM (blue), JJA (green), and SON (orange) and seasonal trend (black).

3.4 Specific Humidity and Wind

As moisture transport is defined by both specific humidity, q , and the wind, \mathbf{v} , the changes in these variables between warm phase and cool phase PDO are also of great interest. The vertical integrations of q (which yields precipitable water, PW) and of \mathbf{v} (also known as mass flux, MF) are taken from the surface up to 300mb:

$$PW = \frac{1}{g} \int_{sfc}^{300mb} q dp \quad \text{Eq. 3.6,}$$

$$MF = \frac{1}{g} \int_{sfc}^{300mb} \mathbf{v} dp \quad \text{Eq. 3.7.}$$

The highest values of specific humidity in the North Pacific region are found near the tropics and steadily decrease towards the northern areas. Specific humidity in the warm phase PDO decreases throughout much of the North Pacific region including Hawaii and Alaska in winter (Figure 3.17a). In the remaining seasons, it increases in the warm phase over Hawaii and portions of Alaska. In spring, northern Alaska experiences a decrease in specific humidity (Figure 3.17b), and in summer, a decrease occurs in the North Pacific Ocean between Alaska and Hawaii (Figure 3.17c).

The mass flux follows a similar pattern to that of the moisture transport: the wind flows east over Alaska and the western coast of North America but west over Hawaii. In the winter season, the wind speeds in the warm phase decrease over Alaska and Hawaii and increase along the west coast of the United States (Figure 3.18a). For spring, wind speeds are greater throughout the arctic but decrease over Hawaii and Alaska (Figure 3.18b). Wind speeds increase in Alaska and over northern Canada and decrease over

Hawaii in summer (Figure 3.18c). The difference of wind speeds show slower wind speeds in the warm phase over Alaska and Hawaii (Figure 3.18d).

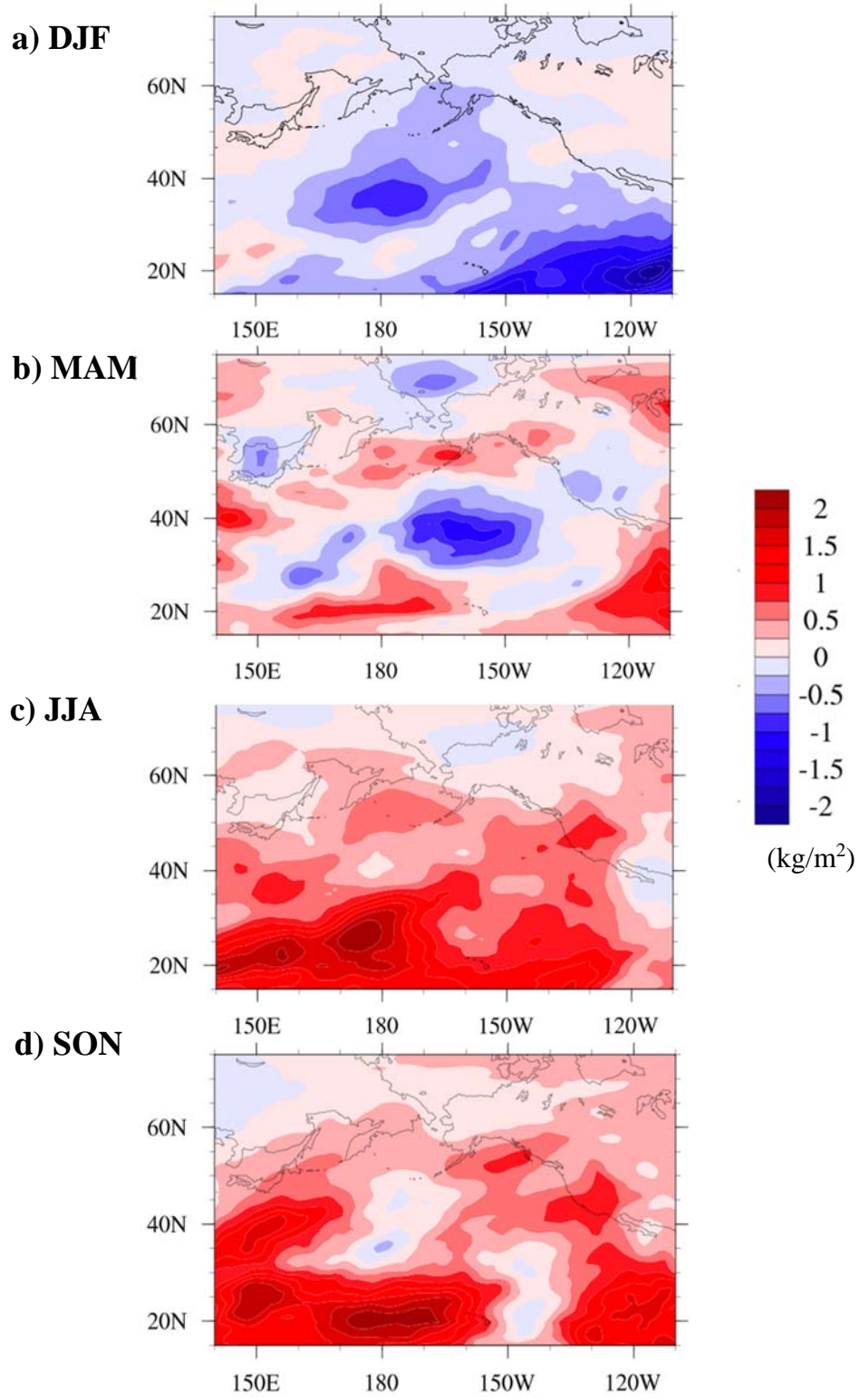


Figure 3.17. PDO difference in precipitable water. Warm phase – cool phase precipitable water is shown for a) DJF, b) MAM, c) JJA, and d) SON.

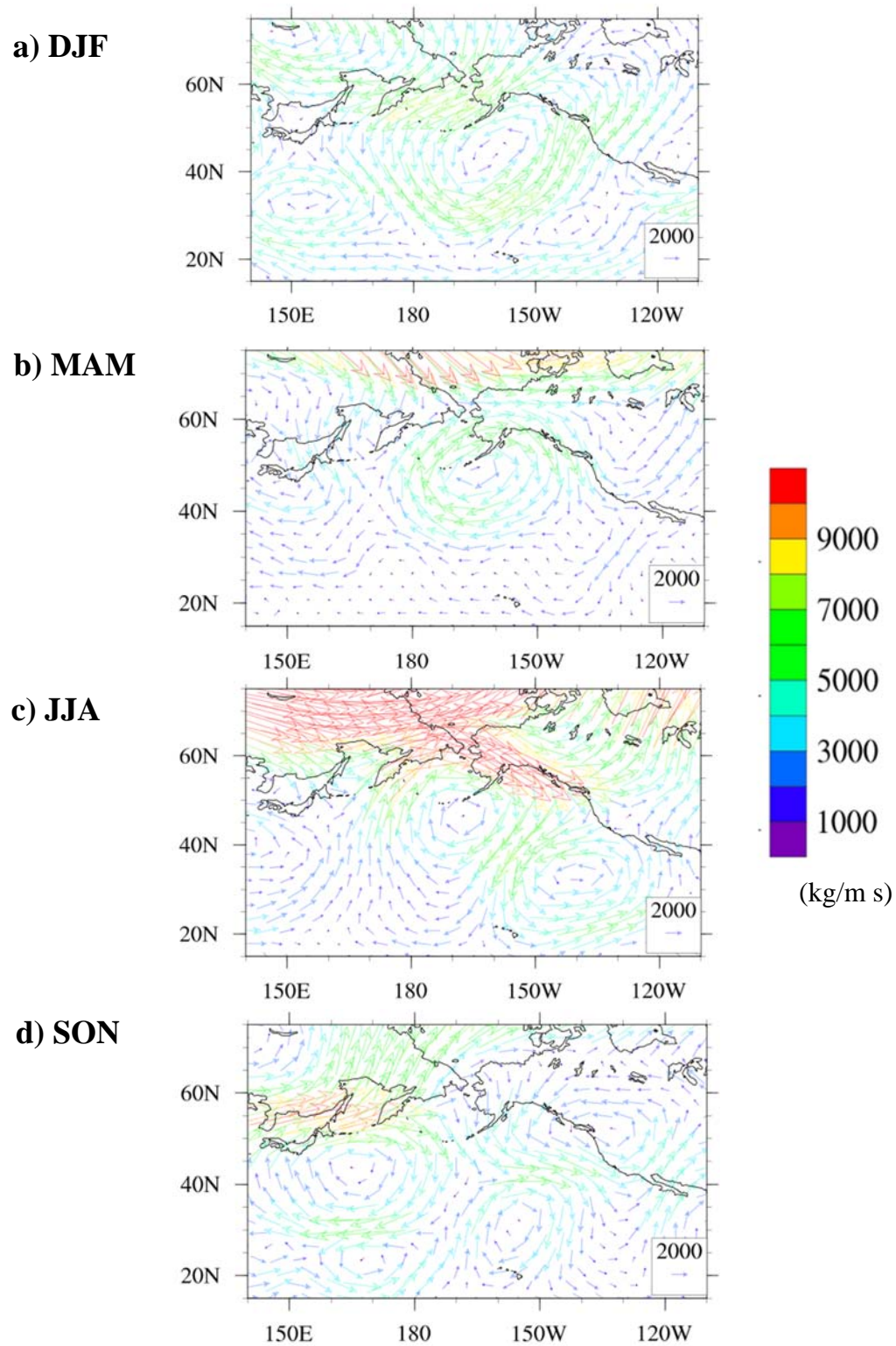


Figure 3.18. PDO difference in mass flux. The difference between warm phase and cool phase mass flux is shown for a) DJF, b) MAM, c) JJA, and d) SON.

3.5 Evaporation

Finally, we look at the evaporation over Alaska and Hawaii during the PDO phases as changes in this process also affect the amount of moisture in the atmosphere. Differences in evaporation are shown in Figure 3.19. Evaporation during warm phase PDO decreases over Hawaii and interior Alaska and increases over the western North Pacific, southwestern Alaska, and the west coast of the United States (Figure 3.19a). In spring (Figure 3.19b), evaporation decreases over arctic Alaska but increases over Hawaii and southern portions of Alaska. Figure 3.19c shows increases in summertime evaporation over arctic Alaska, interior Alaska, and Hawaii. Decreases in evaporation occur over southwestern Alaska in summer. Evaporation in fall (Figure 3.19d) increases over both Alaska and Hawaii and decreases over the western North Pacific.

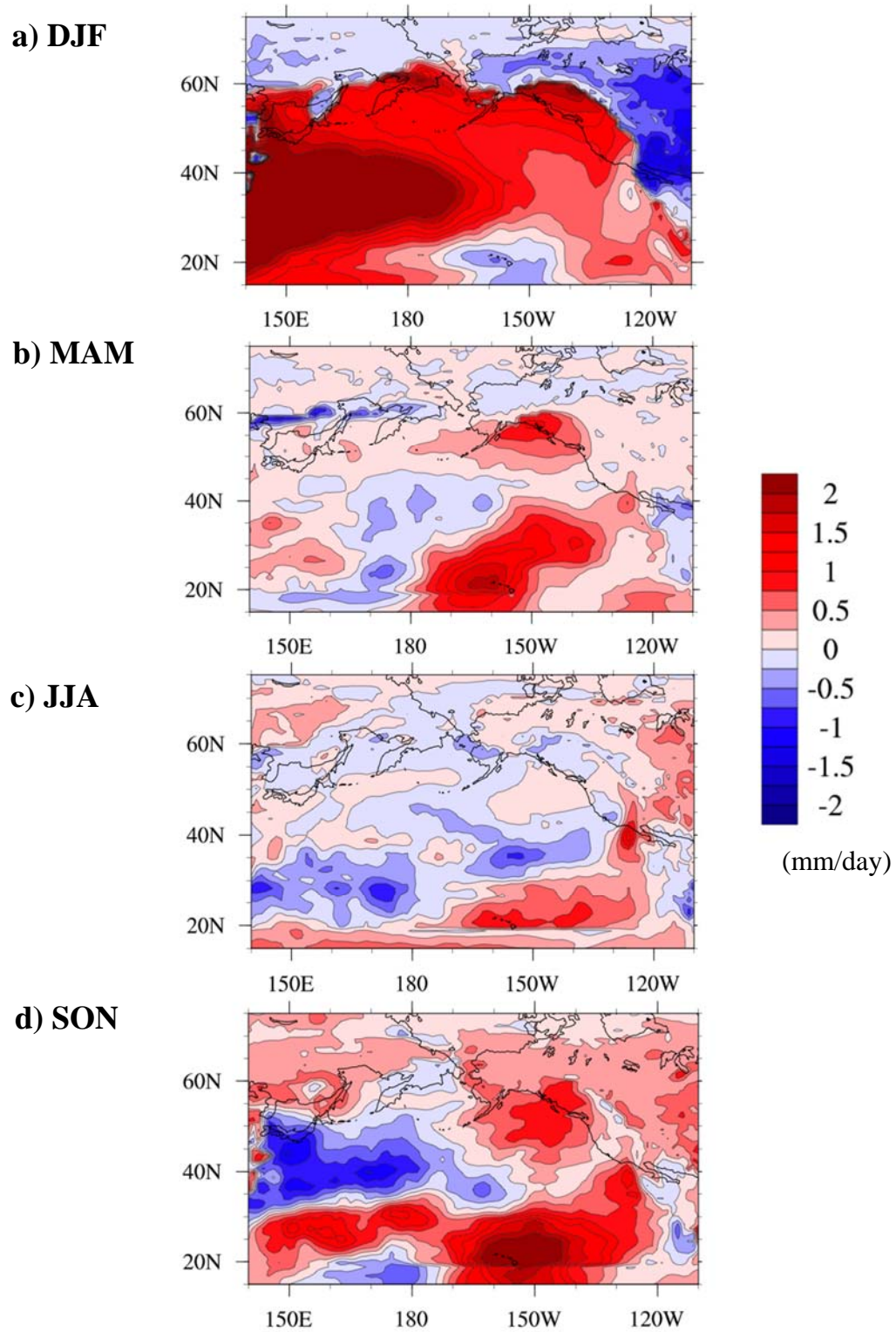


Figure 3.19. PDO difference of evaporation. The difference between warm phase and cool phase mean evaporation is shown for a) DJF, b) MAM, c) JJA, and d) SON.

Chapter 4. Results of the PDO and El Niño Experiment

The PDO provides decadal variability in the North Pacific, but within the separate PDO phases, interannual variability is affected by ENSO SST anomalies. The calculations from Sections 3.1 through 3.4 are repeated for the second experiment in order to determine how the atmospheric moisture transport over the North Pacific between Alaska and Hawaii changes with decadal variabilities due to the PDO phase super-imposed on interannual variabilities like El Niño events and La Niña events.

4.1 Moisture Convergence

The difference between warm phase and cool phase PDO moisture convergence during El Niño events versus La Niña events can be compared in Figures 4.1 and 4.2. While the PDO experiment shows a decrease in moisture convergence in Alaska and Hawaii in winter (Figure 3.6a), this experiment shows an increase during both El Niño and La Niña (Figures 4.1a and 4.2a). Additionally, during La Niña events, moisture convergence is seen to decrease between Alaska and Hawaii and increase during El Niño events. In spring, moisture convergence decreases over Alaska and between Alaska and Hawaii during La Niña (Figure 4.1b) and increases over Alaska and Hawaii during El Niño (Figure 4.2b). Similar to the previous results for summer, moisture convergence increases in arctic Alaska and decreases throughout the rest of Alaska and Hawaii during La Niña (Figure 4.1c). During El Niño (Figure 4.2c), a decrease in moisture convergence is seen over all of Alaska. Decreases in moisture convergence occur in Alaska and Hawaii in fall during both El Niño and La Niña events (Figures 4.1d and 4.2d).

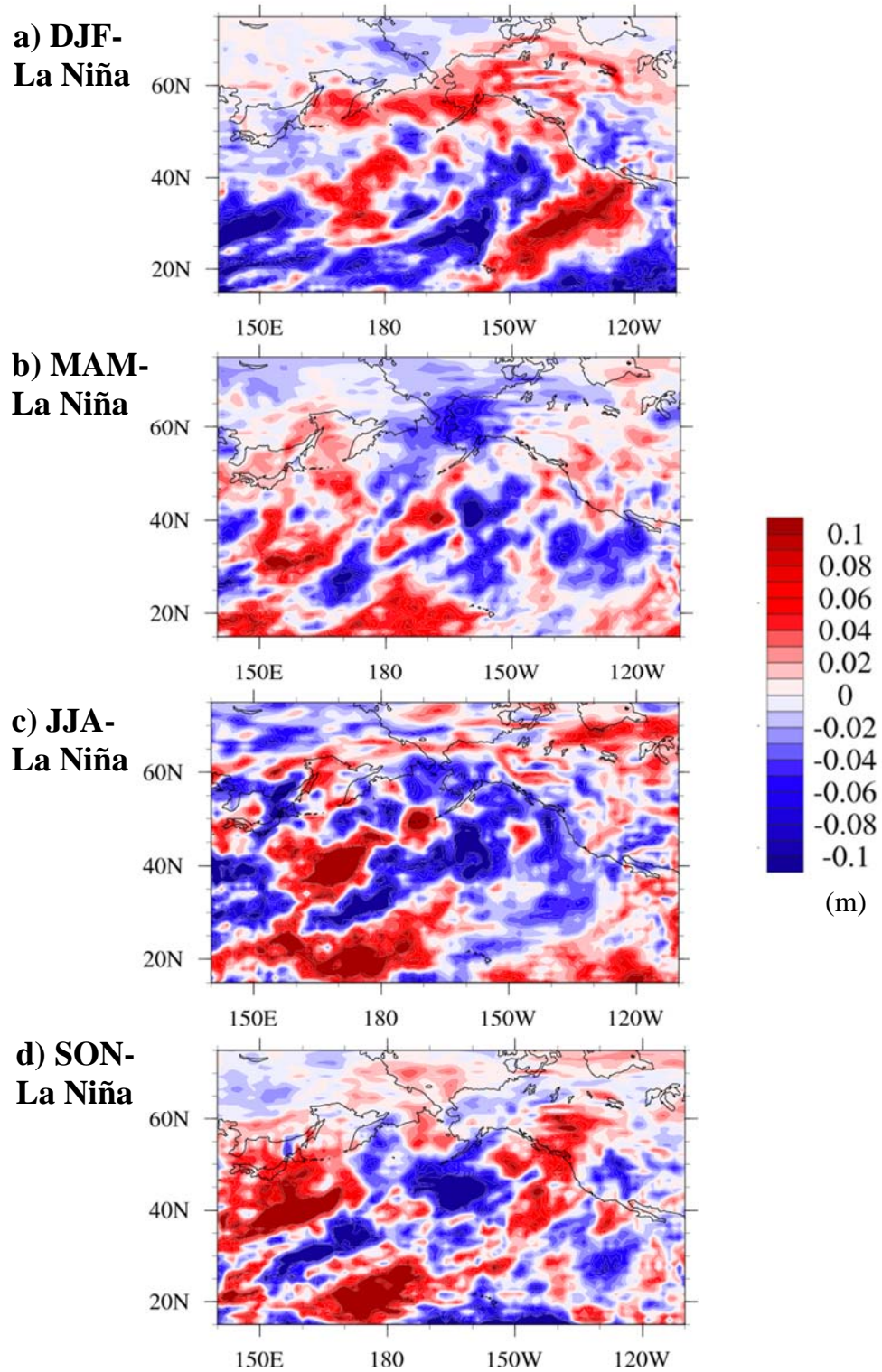


Figure 4.1. PDO difference in moisture convergence during La Niña. The PDO phase difference (warm – cool) in moisture convergence during La Niña events is shown for a) DJF, b) MAM, c) JJA, and d) SON.

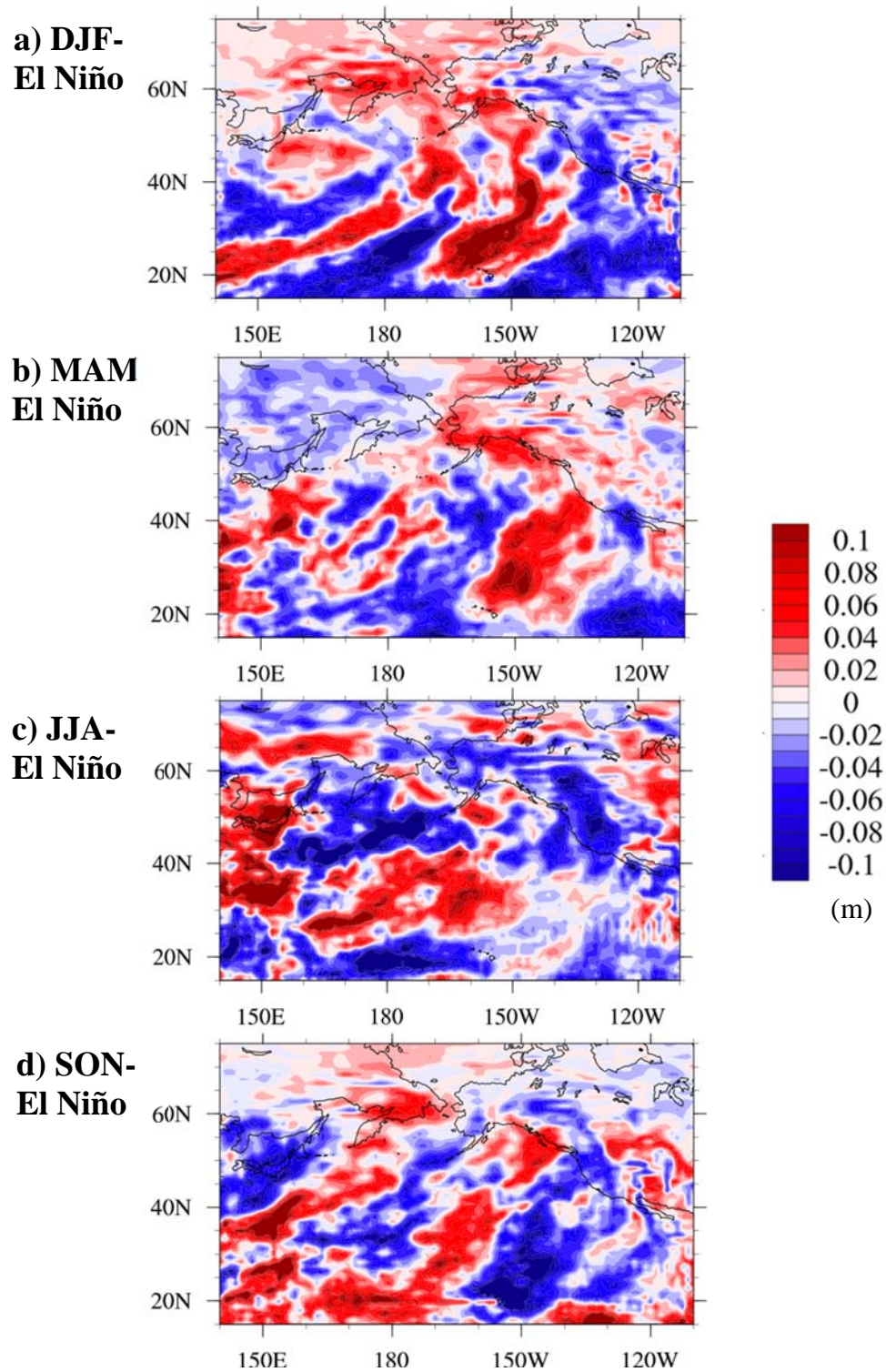
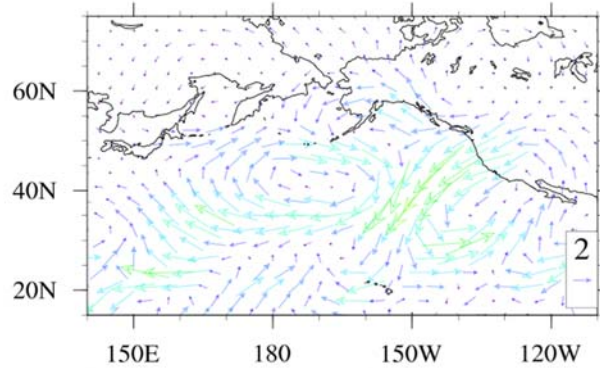


Figure 4.2. PDO difference in moisture convergence during El Niño. The PDO phase difference (warm – cool) in moisture convergence during El Niño events is shown for a) DJF, b) MAM, c) JJA, and d) SON.

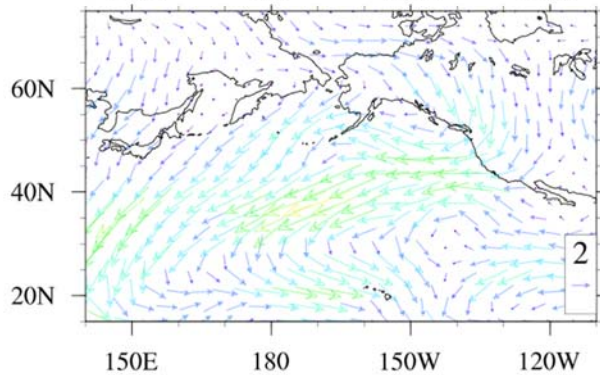
4.2 Moisture Transport

Winter La Niña events show a decrease in transient moisture transport in over Hawaii and Alaska (Figure 4.3a), while winter El Niño events show an increase in Hawaii (Figure 4.4a). The previous results in Section 3.3 showed an increase in both Alaska and Hawaii. The spring and summer changes are similar in that the PDO phase difference of transient moisture transport decreases in Alaska and increases over Hawaii for both El Niño and La Niña (Figures 4.3b and 4.4b, Figures 4.3c and 4.4c), similar to the first experiment. Transient moisture transport increases in western Alaska and Hawaii during fall La Niña events (Figure 4.3d). It increases in Hawaii, the eastern region of Alaska, and the western coast of North America during El Niño events, but decreases in the western portion of Alaska (Figure 4.4d) – similar to the previous results.

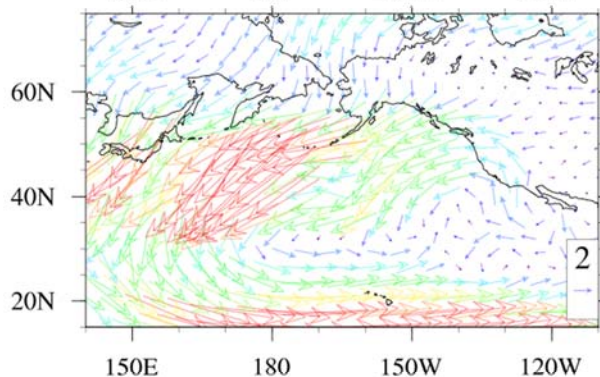
a) DJF-
La Niña



b) MAM-
La Niña



c) JJA-
La Niña



d) SON-
La Niña

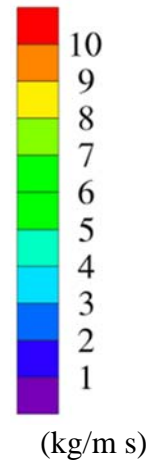
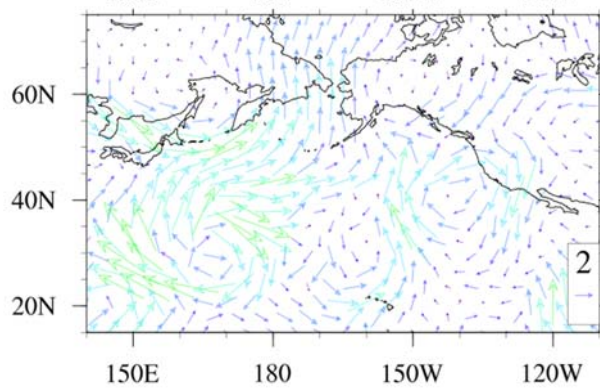


Figure 4.3. PDO difference in transient moisture transport during La Niña. The PDO phase difference (warm – cool) in transient moisture transport during La Niña events is shown for a) DJF, b) MAM, c) JJA, and d) SON.

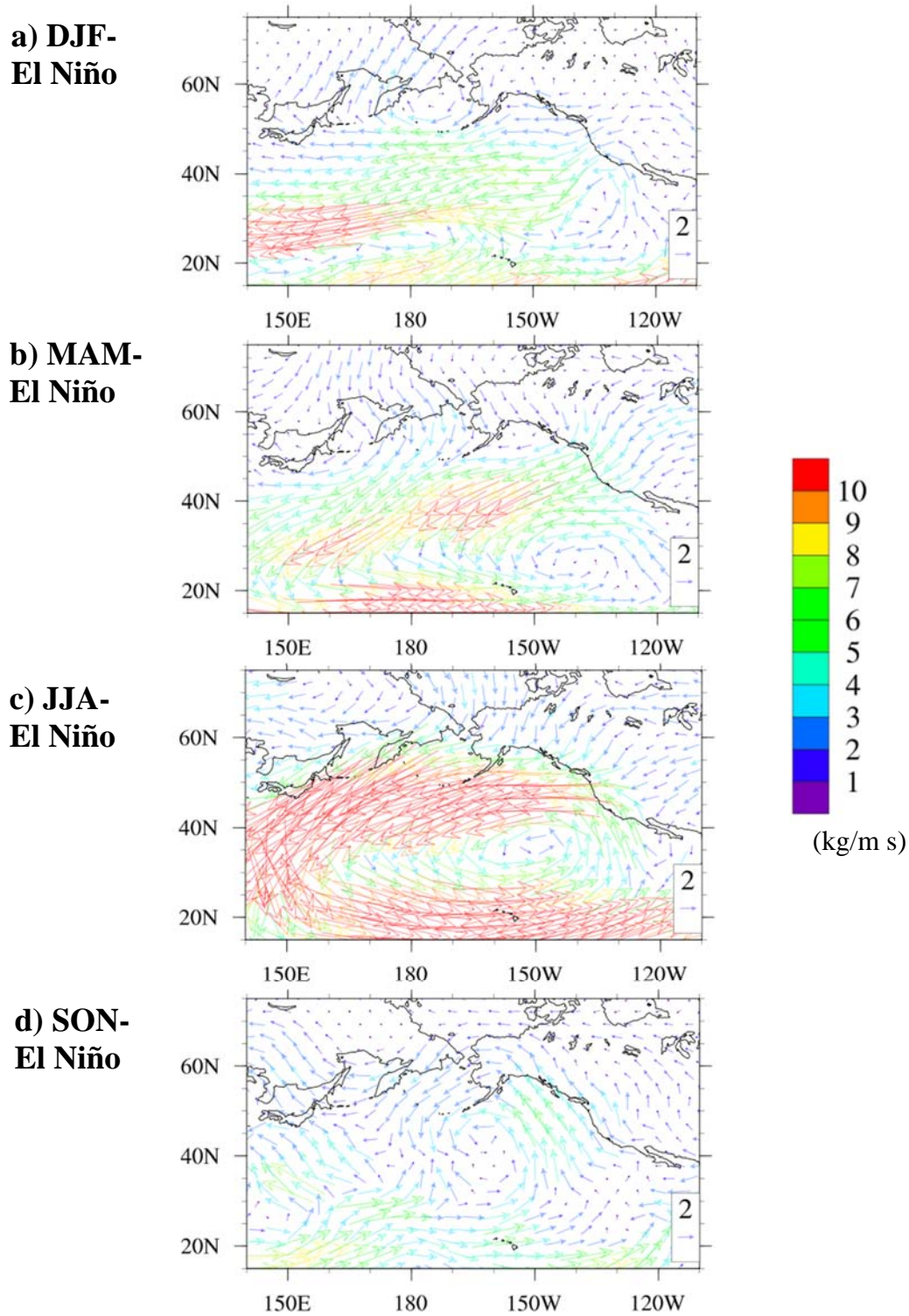


Figure 4.4. PDO difference in transient moisture transport during El Niño. The PDO phase difference (warm – cool) in transient moisture transport during El Niño events is shown for a) DJF, b) MAM, c) JJA, and d) SON.

4.3 Specific Humidity and Wind

Precipitable water slightly decreases in northern Alaska and northern Hawaii and increases in southern Alaska and southern Hawaii during La Niña events in winter (Figure 4.5a). Figures 4.5b and 4.5c show decreases throughout much of the North Pacific during La Niña events in spring and summer. Slight increases in precipitable water occur in fall over Alaska and Hawaii during La Niña events as well (Figure 4.5d). All four seasons see increases from cool phase PDO to warm phase PDO in precipitable water over Alaska, Hawaii, and most of the North Pacific region for El Niño events (Figures 4.6a – 4.6d).

Mass flux increases over Alaska, Hawaii, and the west coast of North America during La Niña in winter (Figure 4.7a). This pattern shifts east during El Niño events so that western Alaska and Hawaii sees increases in mass flux, but it decreases along the west coast of North America (Figure 4.8a). This is not similar to the previous results in Section 3.4 as they show a decrease over Alaska and Hawaii during PDO phase shifts from cool to warm. In spring La Niña events (Figure 4.7b), mass flux decreases over both Alaska and Hawaii and then increases over the same areas during El Niño events (Figure 4.8b). Summer La Niña events show an increase over Alaska and a slight increase over Hawaii (Figure 4.7c), whereas El Niño events show a slight decrease of mass flux over Alaska and a slight increase over Hawaii (Figure 4.8c). In winter, mass flux decreases over Alaska during La Niña events and increases over northwest Canada (Figure 4.7d), but increases over Alaska and decreases over Hawaii during El Niño (Figure 4.8d).

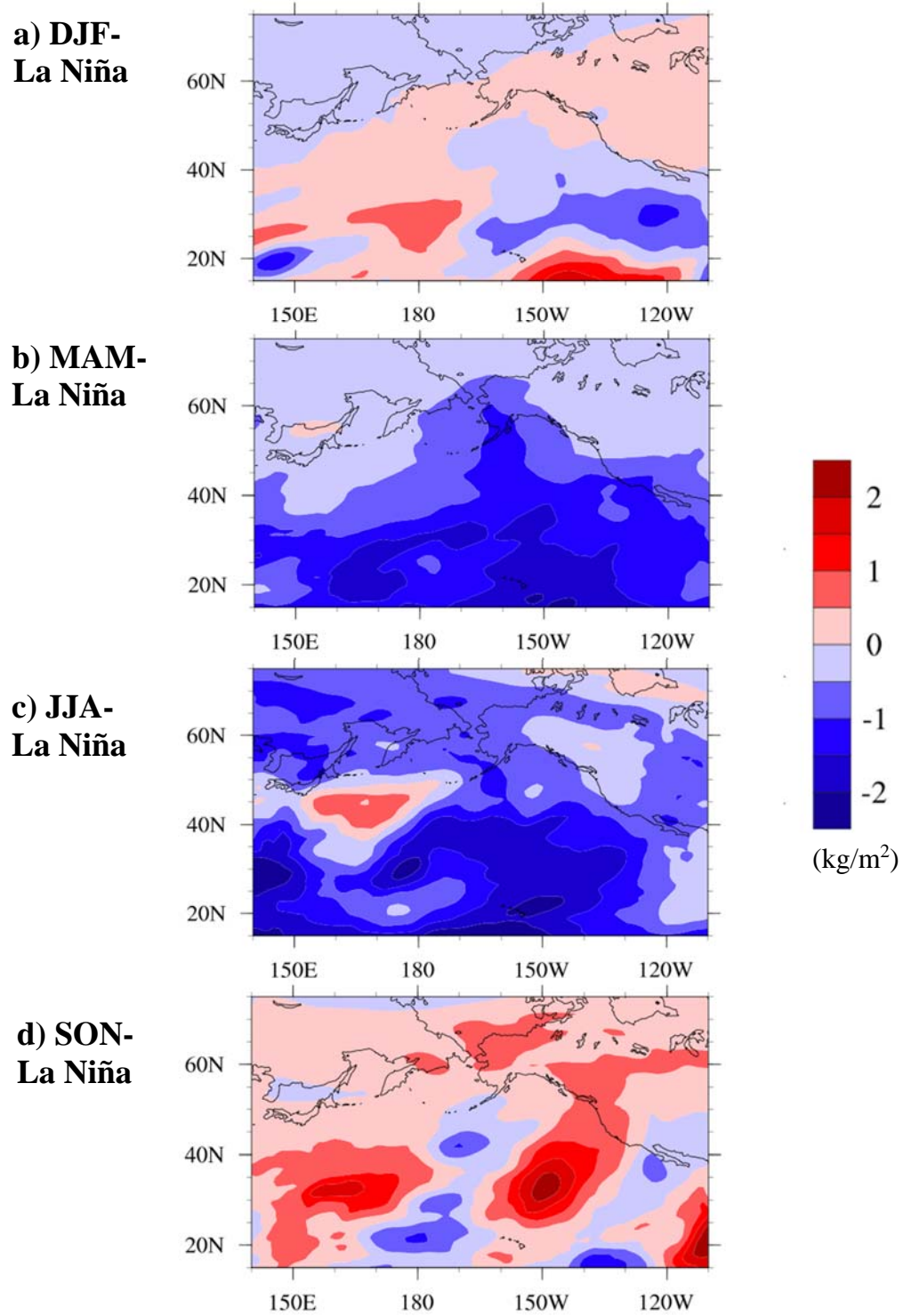


Figure 4.5. PDO difference in precipitable water during La Niña. The PDO phase difference (warm – cool) in precipitable water during La Niña events is shown for a) DJF, b) MAM, c) JJA, and d) SON.

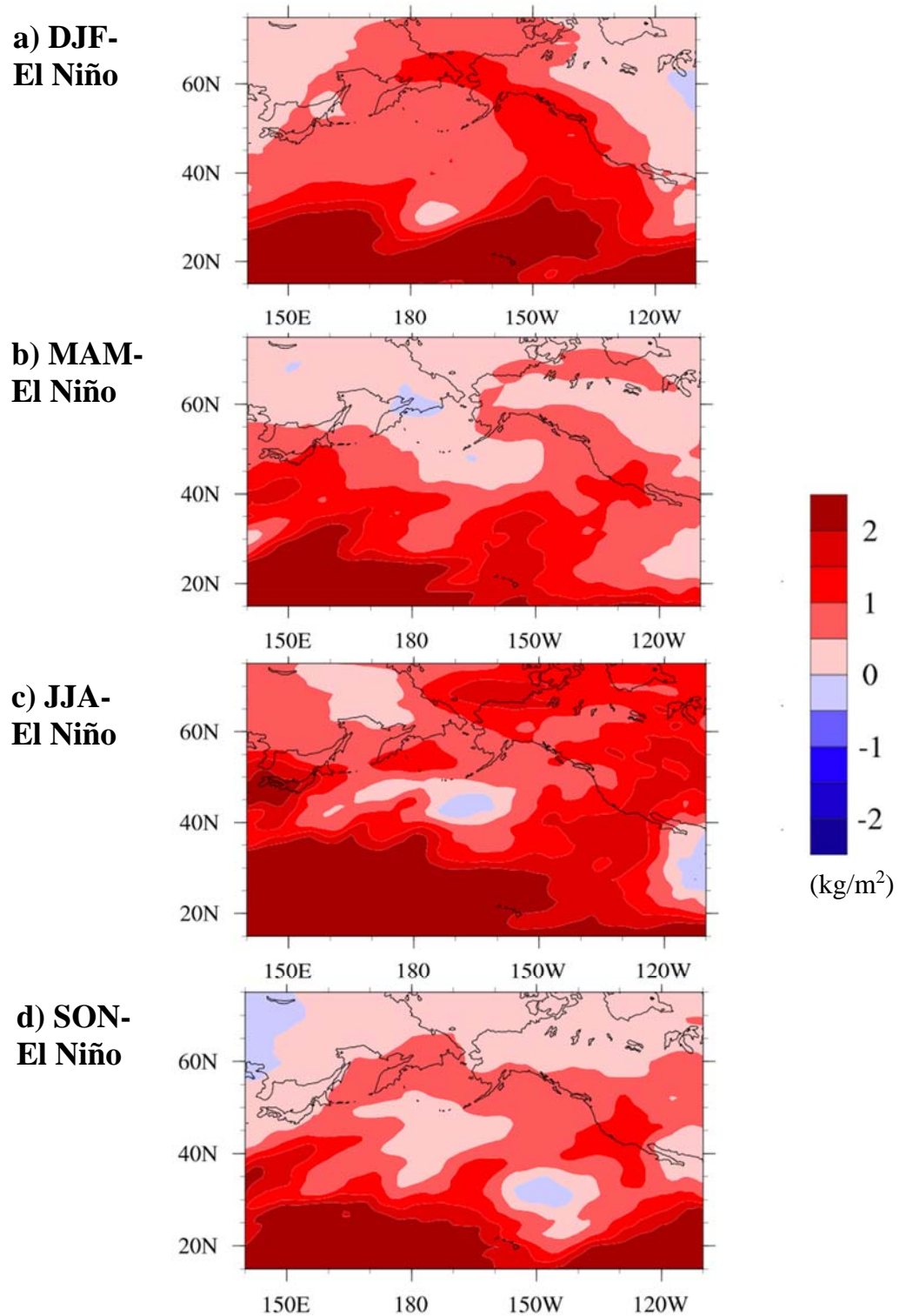


Figure 4.6. PDO difference in precipitable water during El Niño. The PDO phase difference (warm – cool) in precipitable water during El Niño events is shown for a) DJF, b) MAM, c) JJA, and d) SON.

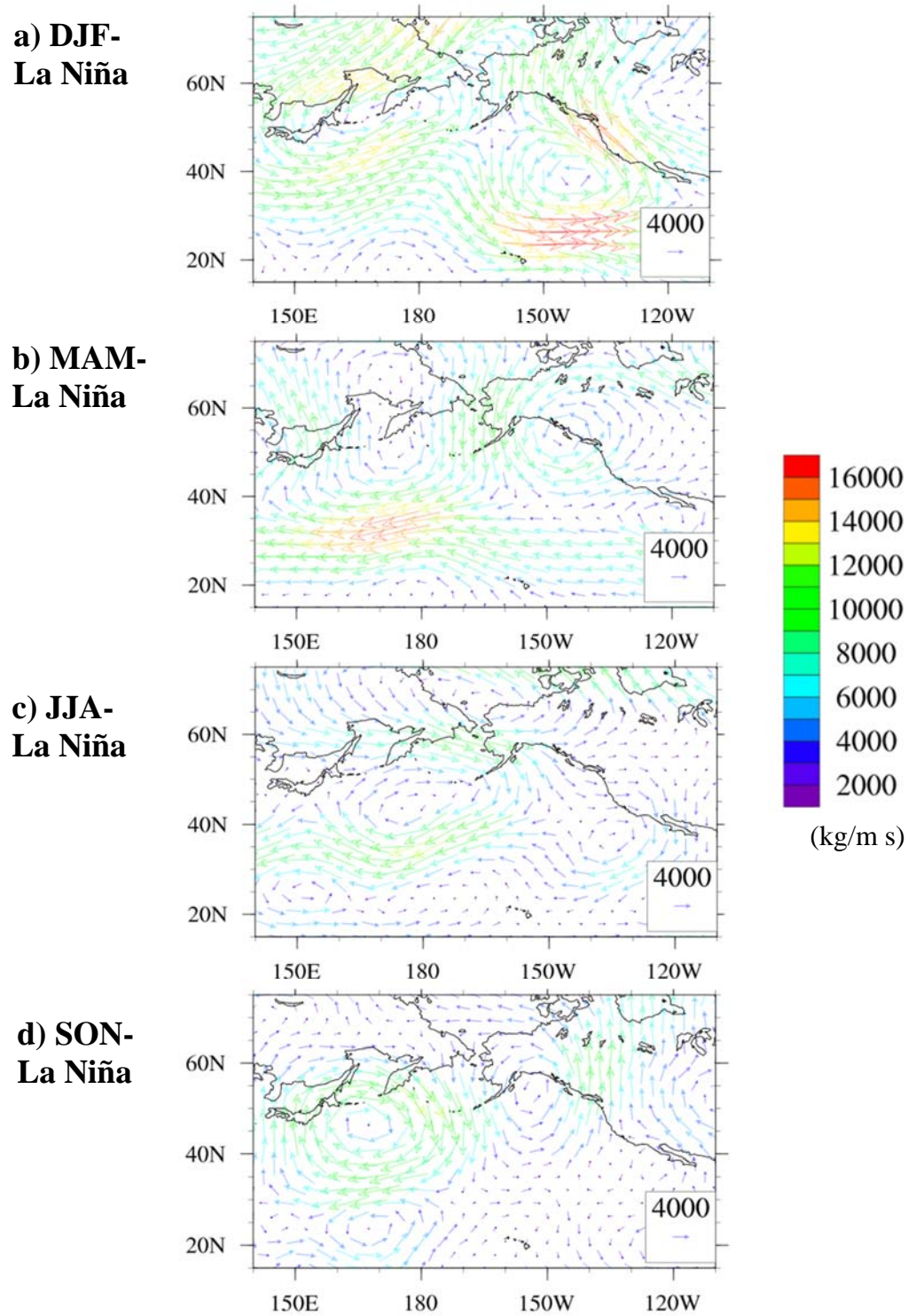


Figure 4.7. PDO difference in mass flux during La Niña. The PDO phase difference (warm – cool) in mass flux during La Niña events is shown for a) DJF, b) MAM, c) JJA, and d) SON.

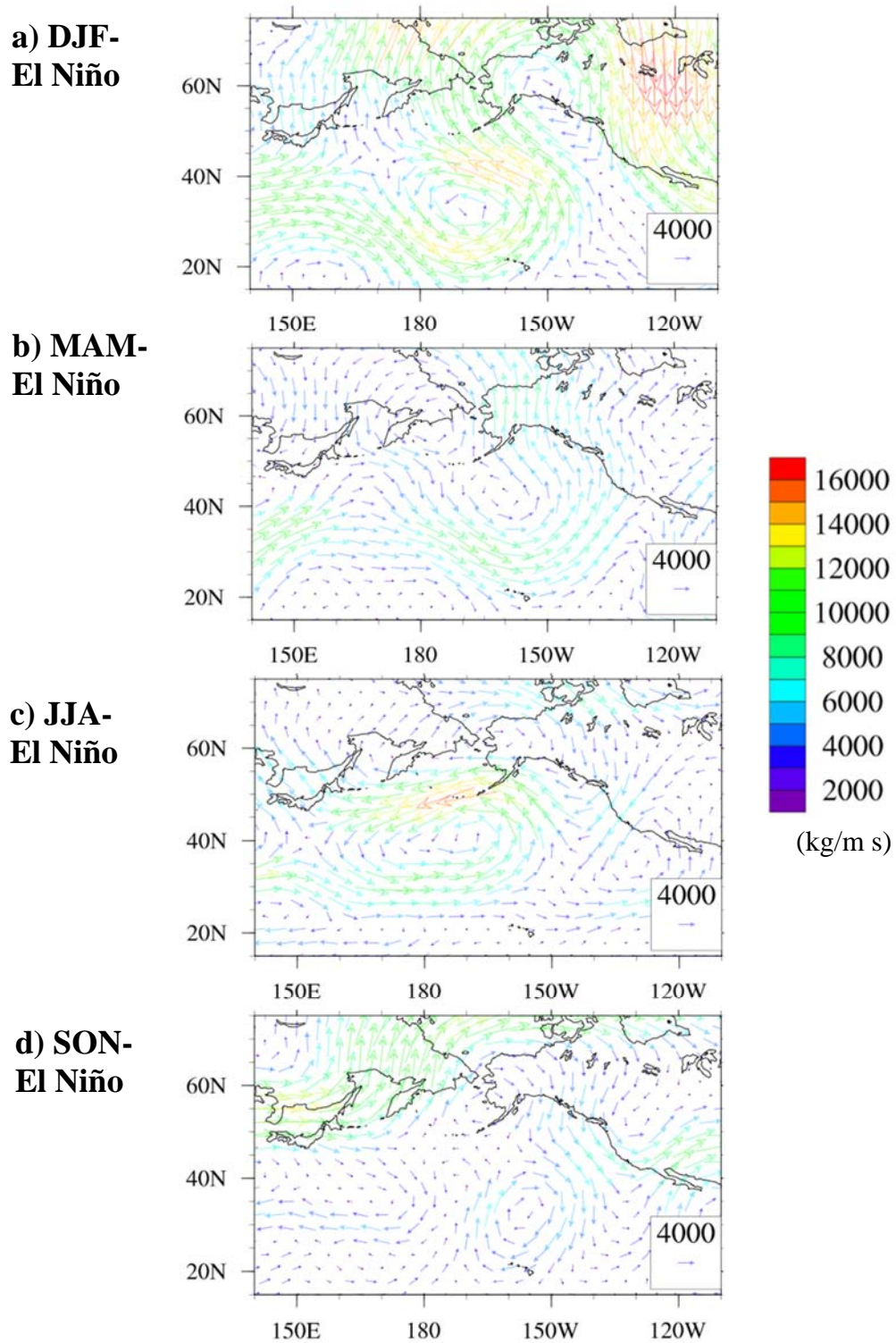


Figure 4.8. PDO difference in mass flux during El Niño. The PDO phase difference (warm – cool) in mass flux during El Niño events is shown for a) DJF, b) MAM, c) JJA, and d) SON.

4.4 Evaporation

Figures 4.9 and 4.10 show the warm phase and cool phase PDO difference of seasonal mean evaporation during La Niña events and El Niño events, respectively. Evaporation over Hawaii is slightly greater during warm phase PDO, El Niño events in winter (Figures 4.9a and 4.10a) and in summer (Figures 4.9c and 4.10c). Evaporation over Alaska does not greatly change during La Niña or El Niño. In spring, evaporation is greater over Alaska and Hawaii during La Niña events (Figures 4.9b and 4.10b). Evaporation over the North Pacific is greater during warm phase PDO, El Niño events in fall (Figures 4.9d and 4.10d), but evaporation over Alaska and Hawaii does not notably change.

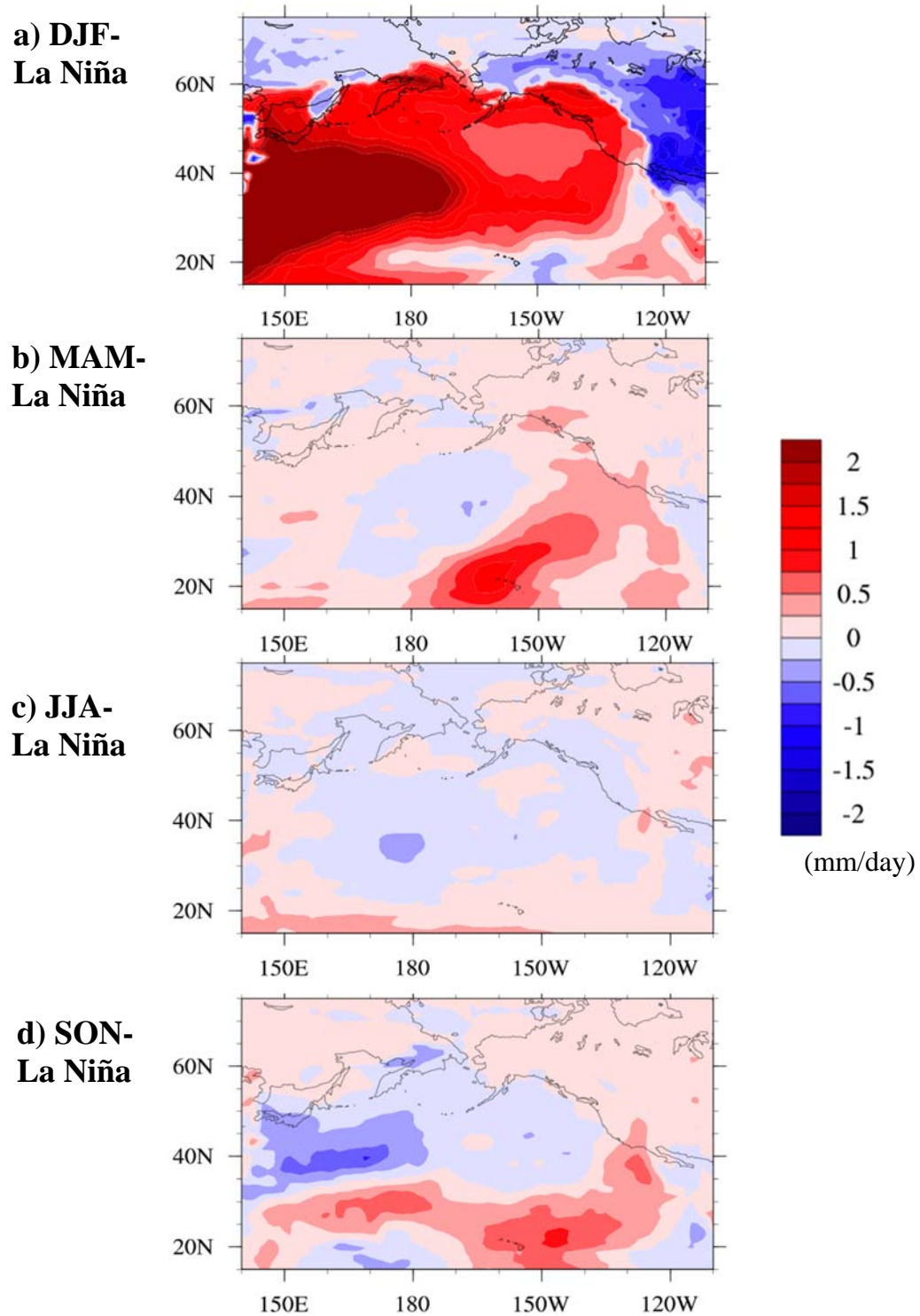


Figure 4.9. PDO difference in evaporation during La Niña. The PDO phase difference (warm – cool) in evaporation during La Niña events is shown for a) DJF, b) MAM, c) JJA, and d) SON.

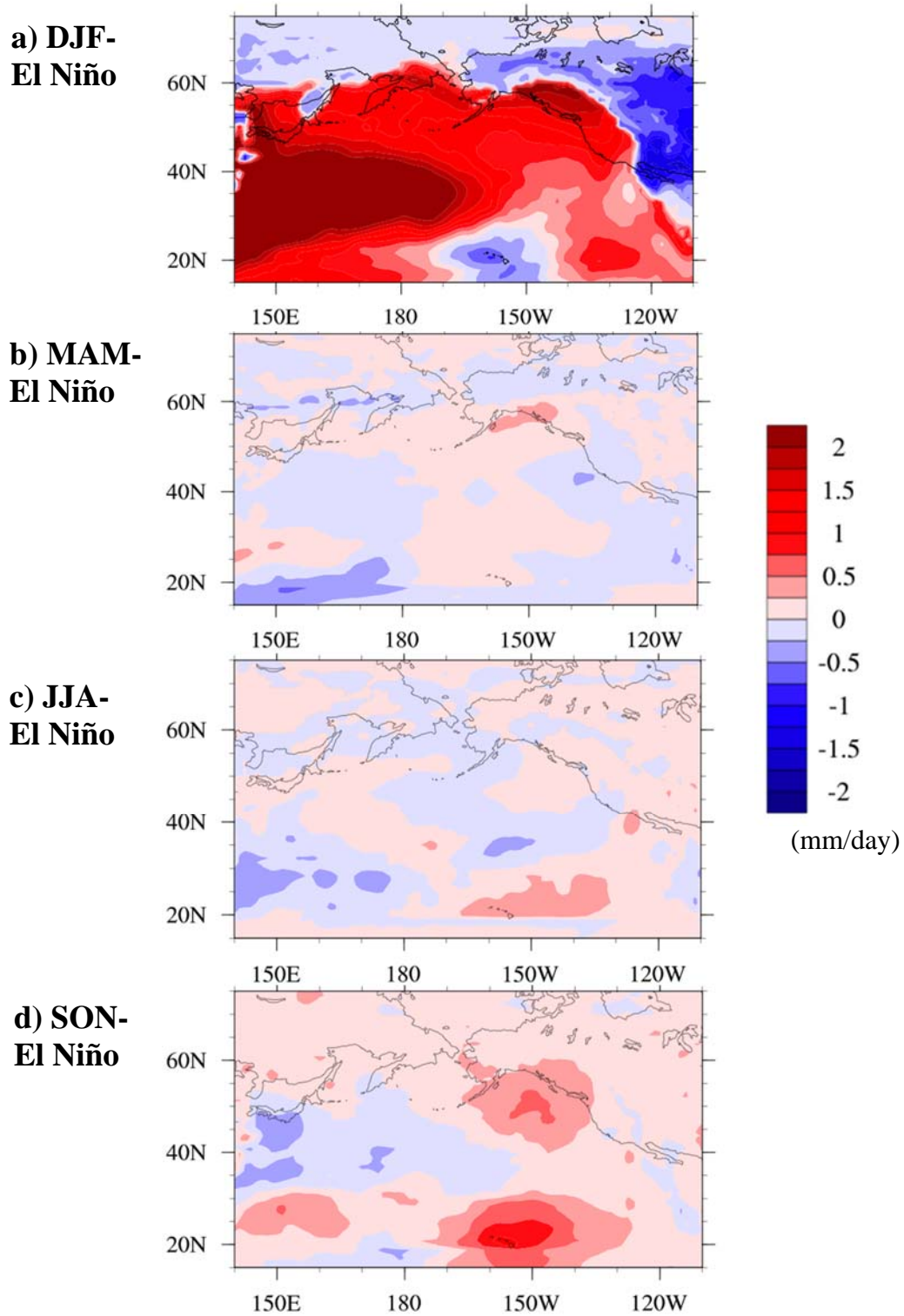


Figure 4.10. PDO difference in evaporation during El Niño. The PDO phase difference (warm – cool) in evaporation during El Niño events is shown for a) DJF, b) MAM, c) JJA, and d) SON.

Chapter 5. Summary and Conclusions

Over the region of the North Pacific Ocean, areas of increased (decreased) moisture convergence correspond to areas of large increases (decreases) in specific humidity as well as increases (decreases) in wind speeds. In areas where the changes in specific humidity are small, the differences in wind speeds affect the change in moisture convergence. Differences in convergence are very small over portions of Alaska and Hawaii – which could account for the fact that changes in moisture convergence do not agree with the observed changes in precipitation. This is most likely due to the coarse resolution of the model. The model topography of Alaska (Figure 5.1) does not capture the real topography (Figure 5.2). For example, the Brooks Range in Northern Alaska has a maximum height of 2,700m, but the model shows maximum heights of 800-1,000m. The model topography also does not capture the changes in elevation due to volcanic mountains in Hawaii (not shown). This difference in model topography exacerbate the disagreement between point source measures.

Net moisture transport into Alaska, calculated from the sum of the moisture transport across four boundary lines, decreases during warm phase PDO in spring and fall, increases in winter, and does not change in summer. These changes are primarily due to the fluctuations of moisture transport along the southern boundary of Alaska as the greatest amounts of moisture entering Alaska occur over that boundary. Conversely, the greatest amounts of moisture leaving Alaska occur over the northern boundary. Moisture leaving along this boundary also increases during warm phase PDO in all seasons except winter.

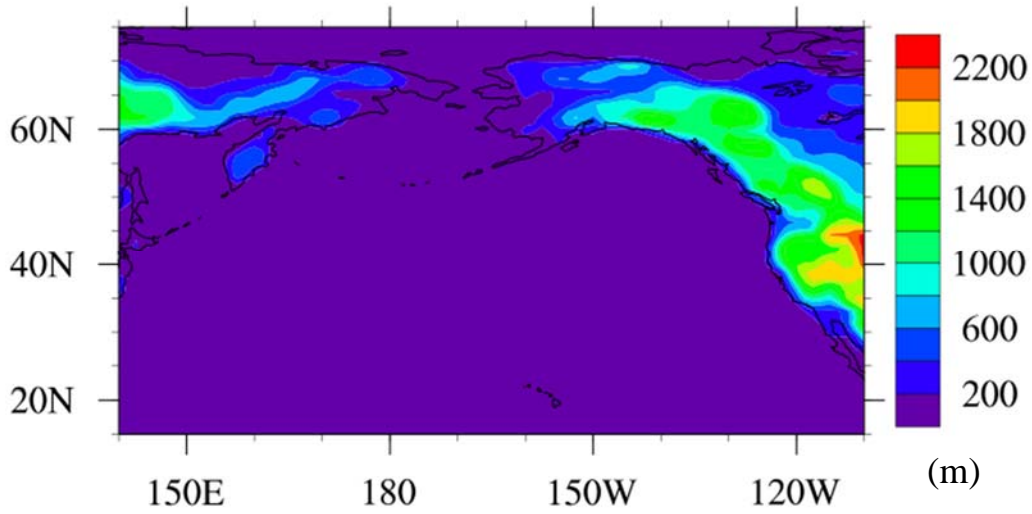


Figure 5.1. Model topography over the North Pacific Ocean.



Figure 5.2. Topography of Alaska. Figure credit: http://www.lksd.org/alaska_in_maps/html/c124.htm

By decomposing the moisture transport into its two components, precipitation is found to be affected by the combination of an increase (or decrease in northern Alaska) in specific humidity during warm PDO phases as well as a decrease in the wind speed over Alaska and Hawaii for most seasons. Therefore, while the amount of moisture in the atmosphere has increased, the winds are not transporting it throughout the North Pacific as quickly, and so the moisture in the atmosphere is able to precipitate out before leaving the local area. Moreover, differences in specific humidity during warm phase PDO can be explained by corresponding changes in evaporation amounts, indicating that evaporation increases have an effect on warm phase PDO precipitation.

The increases in specific humidity over Alaska agree with the previous modeling results of Higgins and Cassano (2009) which showed that increases in precipitation in the Arctic were due primarily to increased atmospheric moisture content. Increases in warm phase PDO evaporation can also be explained by the increases in atmospheric temperatures during warm phase PDO found by Mantua and Hare (2002) and Hartmann and Wendler (2005).

When taking into account interannual variability from global forcing, the differences in moisture convergence over Alaska and between Alaska and Hawaii are greater between warm phase PDO El Niño and La Niña events than between just cool phase and warm phase PDO. The transient moisture transport over Alaska decreases during El Niño compared to La Niña during most seasons (winter, spring, and summer) and increases over Hawaii in all seasons. Specific humidity throughout the North Pacific increases during warm phase PDO and El Niño events but decreases during warm phase PDO and La Niña

events. The wind speeds also change between warm phase La Niña and El Niño with decreases (increases) over Alaska in winter and summer (spring and fall) and over Hawaii in fall (spring and summer). Evaporation does not greatly change over the North Pacific Ocean during El Niño and La Niña, but slight increases are seen over Hawaii during winter, warm phase PDO, El Niño events and over Alaska and Hawaii during spring, warm phase PDO, La Niña events.

Precipitation is an important component to support life around the world, and as such the need to understand its natural variability is also of great importance. Changes in precipitation can have serious effects on human society and natural ecosystems. Significant increases in precipitation can cause widespread flooding along low-lying coastal communities or in mountain valleys, particularly in Alaska in the warming spring months when extra precipitation combines with snow and ice melt leading to flooding. Significant decreases in precipitation in already dry areas like Alaska and the southwestern United States can leave the land too dry and vulnerable to widespread forest fires. The impacts especially have consequences in the remote areas of Alaska as residents may not have immediate access to roads or supplies during emergencies.

While understanding the natural variability of precipitation will not prevent these disasters from occurring, the damage which they cause can be lessened with proper education and preparation. Further research is needed to investigate how these changes in atmospheric moisture transport and moisture convergence due to the PDO phases affect the strength and duration of precipitation events as well as the impacts of increased global air temperatures and carbon dioxide concentrations on the natural variability of

precipitation in the North Pacific.

Ongoing research is vital to complete our understanding of the effects of natural variability on precipitation so that preventative methods can be established and preparations can be made to lessen the impact of such disasters.

References

- Garza, J. A., Chu, P.-S., Norton, C. W., & Schroeder, T. A. (2012). Changes of the prevailing trade winds over the islands of Hawaii and the North Pacific. *Journal of Geophysical Research*, 117, D11109. doi:10.1029/2011JD016888.
- Hartmann, B. & Wendler, G. (2005). The significance of the 1976 Pacific climate shift in the climatology of Alaska. *Journal of Climate*, 18, 4824–4839.
doi: <http://dx.doi.org/10.1175/JCLI3532.1>
- Higgins, M. E., & Cassano, J. J. (2009). Impacts of reduced sea ice on winter arctic atmospheric circulation, precipitation, and temperature. *Journal of Geophysical Research*, 114, D16107. doi:10.1029/2009JD011884.
- Hurrell, J. W., Hack, J. J., Shea, D., Caron, J. M., & Rosinski, J. (2008). A new sea surface temperature and sea ice boundary dataset for the community atmosphere model. *Journal of Climate*, 21(19), 5145-5153.
- Lin, S.-J. & Rood, R. B. (1996). Multidimensional flux-form semi-Lagrangian transport schemes. *Monthly Weather Review*, 124, 2046-2070.
- Lin, S.-J. & Rood, R. B. (1997). An explicit flux-form semi-Lagrangian shallow water model on the sphere. *Quarterly Journal of the Royal Meteorological Society*, 123,

2531-2533.

Mantua, N. J., Hare, S. R., Zhang, Y., Wallace, J. M., & Francis, R. C. (1997). A Pacific decadal climate oscillation with impacts on salmon. *Bulletin of the American Meteorological Society*, 78, 1069-1079.

Mantua, N. J. & Hare, S. R. (2002). The Pacific decadal oscillation. *Journal of Oceanography*, 58 (1), 35-44.

Molders, N. & Kramm, G. (2007). Influence of wildfire induced land-cover changes on clouds and precipitation in interior Alaska – a case study. *Atmospheric Research*, 84, 42-168. doi:10.1016/j.atmosres.2006.06.004.

Molders, N. & Olson, M. A. (2004). Impact on urban effects on precipitation in high latitudes. *Journal of Hydrometeorology*, 5, 409-429.

Neale, R. B. et al. (2010), Description of the NCAR community atmosphere model (CAM5.0). Technical report, NCAR/TN-486+STR, National Center for Atmospheric Research.

Papineau, J. M. (2001). Wintertime temperature anomalies in Alaska correlated with ENSO and PDO. *International Journal of Climatology*, 21, 1577–1592. doi:

10.1002/joc.686.

- Vavrus, S.A., Bhatt, U. S., & Alexeev, V. A. (2011). Factors influencing simulated changes in future arctic cloudiness. *Journal of Climate*, 24, 4817–4830. doi: 10.1175/2011JCLI4029.1.
- Wetherald, R. T., & Manabe, S. (2002). Simulation of hydrologic changes associated with global warming. *Journal of Geophysical Research*, 107(D19), 4379. doi:10.1029/2001JD001195.
- Yarker, M. B., PaiMazumder, D., Cahill, C. F., Dehn, J., Prakash, A., & Molders, N. (2010). Theoretical investigations on potential impacts of high-latitude volcanic emissions of heat, aerosols and water vapor and their interactions with clouds and precipitation. *The Open Atmospheric Science Journal*, 4, 23-44.
- Zhang, J. & Walsh, J.E. (2006). Thermodynamic and hydrological impacts of increasing greenness in northern high latitudes. *Journal of Hydrometeorology*, 7, 1147-1163.
- Zhang, X., He, J., Zhang, J., Polaykov, I., Gerdes, R., Inoue, J., & Wu, P. (2013). Enhanced poleward moisture transport and amplified northern high-latitude wetting trend. *Nature Climate Change*, 3, 47-51. doi: 10.1038/NCLIMATE1631.